ISSN 0736-5306

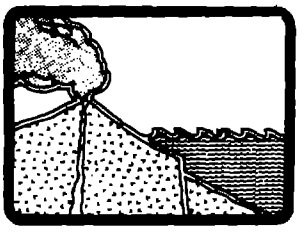

SCIENCE OF TSUNAMI HAZARDS

The International Journal of The Tsunami Society

Volume 9 Number 2 1991

AN INVESTIGATION OF TWO TSUNAMIS RECORDED AT ADAK, ALASKA 67
ZYGMUNT KOWALIK
University of Alaska, Fairbanks, Alaska, USA
PAUL M. WHITMORE
Alaska Tsunami Warning Center, Palmer, Alaska, USA

MODELING HILO, HAWAII TSUNAMI INUNDATION 85
CHARLES L. MADER and GEORGE CURTIS
University of Hawaii, Honolulu, USA

SOURCE PARAMETERS OF DESTRUCTIVE TSUNAMIS 95
AUGUSTINE S. FURUMOTO
University of Hawaii, Honolulu, Hawaii, USA

ANALYTICAL THEORY FOR TSUNAMI RUN UP ON A SMOOTH SLOPE 115
V. M. KAISTRENKO, R. Kh. MAZOVA, E. N. PELINOVSKY AND K. V. SIMONOV
Institute of Applied Physics, Gorky, USSR

OBJECTIVE: The Tsunami Society publishes this journal to increase and disseminate knowledge about tsunamis and their hazards.

DISCLAIMER: The Tsunami Society publishes this journal to disseminate information relating to tsunamis. Although these articles have been technically reviewed by peers, The Tsunami Society is not responsible for the veracity of any statement, opinion, or consequences.

Submit manuscripts of articles, notes, or letters to:

T. S. Murty Technical Editor
Institute of Ocean Sciences
Department of Fisheries and Oceans
Sidney, B.C., Canada V8L 4B2

If article is accepted for publication the author(s) must submit a camera ready manuscript. A voluntary $50.00 page charge will include 50 reprints.

SUBSCRIPTION INFORMATION: Price per copy $20.00 USA

ISSN 0736-5306

Published by The Tsunami Society in Honolulu, Hawaii, U.S.A.

An Investigation of Two Tsunamis Recorded at Adak, Alaska

Zygmunt Kowalik
Institute of Marine Science
University of Alaska, Fairbanks
Fairbanks, Alaska 99775-1080

Paul M. Whitmore
Alaska Tsunami Warning Center
910 S. Felton St.
Palmer, Alaska 99645

ABSTRACT

Tsunamis generated from the 1952 Kamchatka earthquake and the 1986 Andreanof Islands earthquake are modeled and compared to recordings at Adak, Alaska. Non-linear, shallow water equations which include Coriolis and friction forces are solved with a finite difference scheme to generate and propagate the tsunami. Tsunami propagation over long distances requires solution of a large system of equations. Therefore, we used a computational grid with different grid sizes over different geographical domains. This approach reduces computational effort and allows to increase spatial resolution in the shelf area. The numerical problems which occur at the boundary between two grids are briefly discussed and formulas for the grid interaction are given.

The two modeled tsunamis at Adak compare well with the recorded waves in respect to maximum amplitude and build-up, though the 1986 modeled tsunami period is slightly longer than the recorded period. Inclusion of Coriolis, friction, and non-linear terms in the equations of motion proves to have only a minor effect on the modeled waves. Simulation of a moving rupture versus instantaneous source uplift also has a minor effect on the modeled tsunami.

Introduction

As micro-computers become increasingly faster, numerical modeling of tsunamis gains greater potential to predict wave heights prior to impact on the coast. In this study, we present a method to accurately generate and propagate tsunamis. The method is tested with two tsunamis recorded at Adak, Alaska. These tsunamis, produced by the 1952 Kamchatka and the 1986 Andreanof Islands earthquakes, provide an opportunity to model both a trans-Pacific and a locally generated tsunami. In addition to testing the method, we test the significance of various terms in the equations of motion with the objective of computing an accurate model in the least amount of time. The importance of accounting for moving fault rupture versus instantaneous uplift is also examined.

Tsunami propagation over long distances requires the solution of the equations of motion and continuity at a large number of grid points. An approach which decreases the number of grid points is to subdivide a large computational domain into a few subdomains (Ng *et al.*, 1990). The rationale behind using multiple domains is to reduce computation time by placing a coarse grid over the deep water region and finer grids over the shallower coastal regions. Shuto *et al.* (1985) demonstrated with a one-dimensional model that each tsunami wavelength should be covered by at least 10 to 20 grid points to diminish numerical dispersion (dissipation). This implies that using finer grids in shallow water where tsunami wavelength decreases will prevent either over-defining the deep ocean propagation or under-defining the coastal region computations.

To propagate tsunamis between grids of different spacing, either an interactive or a non-interactive connection can be used. In an interactive connection the tsunami signal passes through the boundary not only from the coarse-grid domain to the fine-grid domain, but in the opposite direction as well (Ramming and Kowalik, 1980). In a non-interactive approach a tsunami travelling from the fine towards the coarse grid will not affect the wave in the coarse grid. In this study both approaches are used. The non-interactive approach is used when connecting a Pacific-wide grid with a grid over the region of interest while still in deep water. The interactive approach is used when connecting a fine grid over the shelf with the deep water grid in the area of interest and again when connecting a super-fine grid over bays and inlets to the fine grid. A detailed approach such as this is important at Adak, Alaska, which is an area of complex bathymetry with multiple entrances connecting local bays to the open ocean.

Numerical Method

The equations of motion and continuity in a spherical coordinate system are used to investigate tsunami generation and propagation. These are (Murty, 1984)

$$\frac{\partial u}{\partial t} + u\frac{\partial u}{R\cos\varphi\,\partial\lambda} + v\frac{\partial u}{R\partial\varphi} - fv = \frac{-g}{R\cos\varphi}\frac{\partial\zeta}{\partial\lambda} - \frac{ru(u^2+v^2)^{1/2}}{(\zeta+H-\eta)} \qquad (1)$$

$$\frac{\partial v}{\partial t} + u\frac{\partial v}{R\cos\varphi\,\partial\lambda} + v\frac{\partial v}{R\partial\varphi} + fu = \frac{-g}{R}\frac{\partial\zeta}{\partial\varphi} - \frac{rv(u^2+v^2)^{1/2}}{(\zeta+H-\eta)} \qquad (2)$$

$$\frac{1}{R\cos\varphi}\left(\frac{\partial(u(\zeta+H-\eta))}{\partial\lambda} + \frac{\partial(v(\zeta+H-\eta))\cos\varphi}{\partial\varphi}\right) = \frac{\partial\eta}{\partial t} - \frac{\partial\zeta}{\partial t}, \qquad (3)$$

where; u is the east-west component of particle velocity, v is the north-south component of particle velocity, ζ denotes variation of sea-level from equilibrium, t is the time, f is the Coriolis parameter ($f=2\omega\sin\varphi$), ω is the angular velocity of the earth's rotation, g is the gravity acceleration ($g=9.81 m/s^2$), R is the radius of the earth, φ is latitude, λ is longitude, η is the bottom displacement, r is the coefficient of bottom friction ($r=0.0033$), and H is water depth prior to source displacement.

To describe energy transfer from the tsunami source to the various locations an energy flux

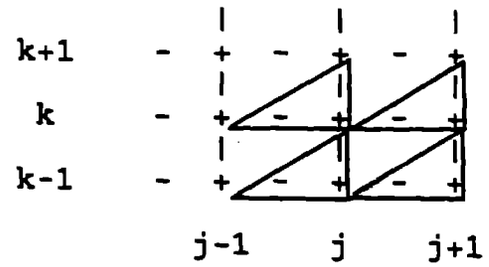

Figure 1. Sea-level is computed at the + points. North-south and east-west velocities are indicated by | and - respectively. The sea-level, north-south velocity, and east-west velocity are organized into triplets and are referenced by the same j,k index.

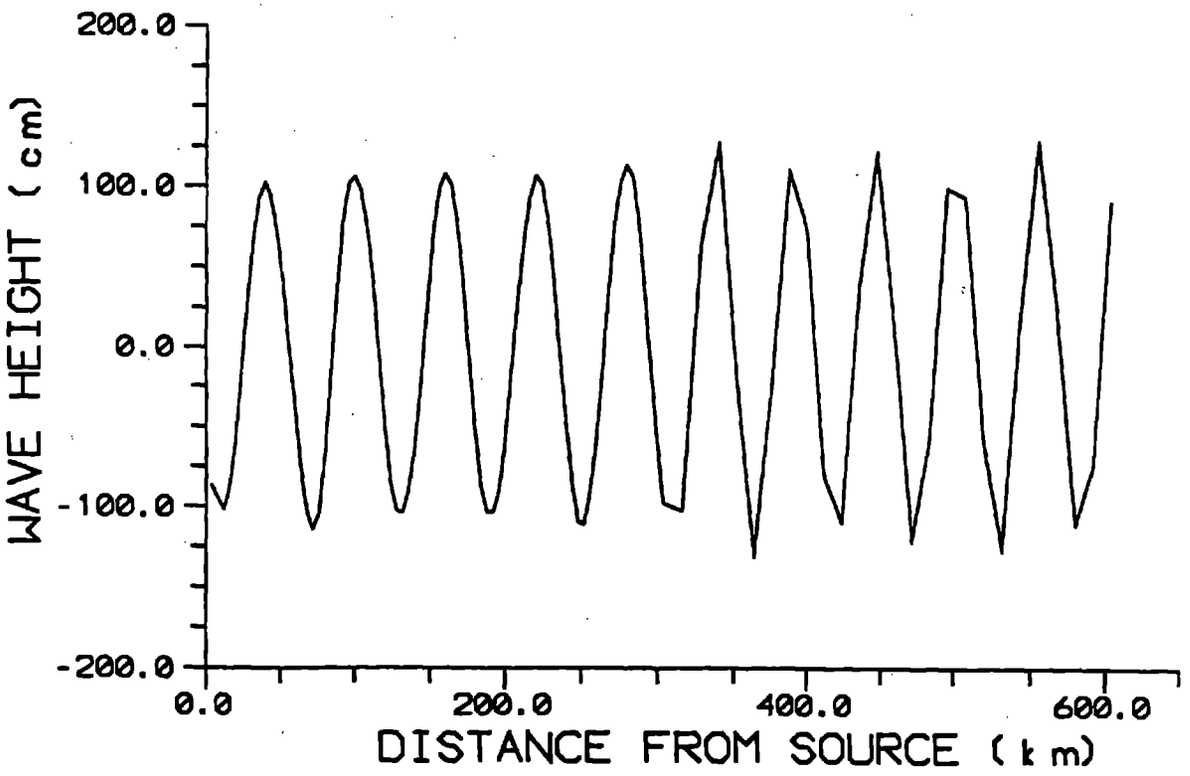

Figure 2. Wave height versus distance from wave generating source 12500s after wave motion begins. The sine wave generated at the left end of a channel propagates to the right end, where the radiation condition is applied. The wave has amplitude 1m, period 600s, wavelength 60km, and speed 100m/s over a flat bottom with depth 1020m. The grid space step from 0 to 300km is 4km (15 pts./wavelength). The space step from 300km to 600km is 12km (5 pts./wavelength). Note the poor numerical approximation over the coarser grid.

vector will be used. This vector characterizes the flux of energy through the unit width surface extended from the surface to the bottom. The components of the vector along latitude and longitude are given by Gill (1982).

$$E_\lambda = \varrho u H((u^2+v^2)/2 + g\zeta) \tag{4}$$

$$E_\varphi = \varrho v H((u^2+v^2)/2) + g\zeta) . \tag{5}$$

Here ϱ is the water density. Usually, in periodical processes the flux vector is taken as an average over wave period; with tsunamis this approach is difficult to realize because of the unknown period. Therefore, we shall construct a field of the maximum energy flux. The magnitude of the energy flux vector, $E = (E_\lambda^2+E_\varphi^2)^{1/2}$, will be compared at the different time steps and the largest value will be retained to depict the maximum energy flux. This will help us to study tsunami source directivity.

An explicit-in-time finite difference scheme is used to solve eqs. (1)-(3) over the area of interest. This scheme solves for the sea-level height and velocities by application staggered space-grid (Fig. 1). In finite difference form eqs. (1)-(3) become

$$\begin{aligned} u_{j,k}^{t} = u_{j,k}^{t-1} &- \frac{T}{R\cos\varphi_k \Delta\lambda}\left(UPOS\left(u_{j,k}^{t-1} - u_{j-1,k}^{t-1}\right) + UNEG\left(u_{j+1,k}^{t-1}\right.\right. \\ &\left.\left. - u_{j,k}^{t-1}\right)\right) - \frac{T}{R\Delta\varphi}\left(VAUP\left(u_{j,k}^{t-1} - u_{j,k-1}^{t-1}\right) + VAUN\left(u_{j,k+1}^{t-1} - u_{j,k}^{t-1}\right)\right) \\ &+ 2T\omega\sin\varphi_k VAU - \frac{gT}{R\cos\varphi_k \Delta\lambda}\left(\zeta_{j,k}^{t-1} - \zeta_{j-1,k}^{t-1}\right) \\ &- \frac{rT}{H1} * u_{j,k}^{t-1} * \left[\left(u_{j,k}^{t-1}\right)^2 + (VAU)^2\right]^{1/2} \end{aligned} \tag{6}$$

$$\begin{aligned} v_{j,k}^{t} = v_{j,k}^{t-1} &- \frac{T}{R\cos\varphi_k \Delta\lambda}\left(UAVP\left(v_{j,k}^{t-1} - v_{j-1,k}^{t-1}\right) + UAVN\left(v_{j+1,k}^{t-1}\right.\right. \\ &\left.\left. - v_{j,k}^{t-1}\right)\right) - \frac{T}{R\Delta\varphi}\left(VPOS\left(v_{j,k}^{t-1} - v_{j,k-1}^{t-1}\right) + VNEG\left(v_{j,k+1}^{t-1} - v_{j,k}^{t-1}\right)\right) \\ &- 2T\omega UAV(\sin\varphi_k + \sin\varphi_{k+1})/2 - \frac{gT}{R\Delta\varphi}\left(\zeta_{j,k+1}^{t-1} - \zeta_{j,k}^{t-1}\right) \\ &- \frac{rT}{H2} * v_{j,k}^{t-1} * \left[\left(v_{j,k}^{t-1}\right)^2 + (UAV)^2\right]^{1/2} \end{aligned} \tag{7}$$

$$\zeta_{j,k}^{t} = \eta_{j,k}^{t} - \eta_{j,k}^{t-1} + \zeta_{j,k}^{t-1} - \frac{T}{R\cos\varphi_k}\left(\frac{u_{j+1,k}^{t} * HJ1 - u_{j,k}^{t} * HJ2}{\Delta\lambda} + \frac{SCP * v_{j,k}^{t} * HK1 - SC * v_{j,k-1}^{t} * HK2}{\Delta\varphi}\right), \tag{8}$$

where

$$UPOS = (u_{j,k}^{t-1} + |u_{j,k}^{t-1}|)/2,$$
$$UNEG = (u_{j,k}^{t-1} - |u_{j,k}^{t-1}|)/2,$$
$$VAUP = (VAU + |VAU|)/2,$$
$$VAUN = (VAU - |VAU|)/2,$$
$$VAU = (v_{j,k}^{t-1} + v_{j-1,k}^{t-1} + v_{j,k-1}^{t-1} + v_{j-1,k-1}^{t-1})/4,$$
$$H1 = MAX(((H_{j,k} + \zeta_{j,k}^{t-1} - \eta_{j,k}^{t}) + (H_{j-1,k} + \zeta_{j-1,k}^{t-1} - \eta_{j-1,k}^{t}))/2), H_{min}),$$
$$H_{min} - minimum\ depth\ allowed\ in\ computation\ (10m),$$
$$UAVP = (UAV + |UAV|)/2,$$
$$UAVN = (UAV - |UAV|)/2,$$
$$VPOS = (v_{j,k}^{t-1} + |v_{j,k}^{t-1}|)/2,$$
$$VNEG = (v_{j,k}^{t-1} - |v_{j,k}^{t-1}|)/2,$$
$$UAV = (u_{j,k}^{t} + u_{j,k+1}^{t} + u_{j+1,k+1}^{t} + u_{j+1,k}^{t})/4,$$
$$H2 = MAX(((H_{j,k} + \zeta_{j,k}^{t-1} - \eta_{j,k}^{t}) + (H_{j,k+1} + \zeta_{j,k+1}^{t-1} - \eta_{j,k+1}^{t}))/2), H_{min}),$$
$$HJ1 = MAX(((H_{j,k} + \zeta_{j,k}^{t-1} - \eta_{j,k}^{t}) + (H_{j+1,k} + \zeta_{j+1,k}^{t-1} - \eta_{j+1,k}^{t}))/2), H_{min}),$$
$$HJ2 = MAX(((H_{j,k} + \zeta_{j,k}^{t-1} - \eta_{j,k}^{t}) + (H_{j-1,k} + \zeta_{j-1,k}^{t-1} - \eta_{j-1,k}^{t}))/2), H_{min}),$$
$$HK1 = MAX(((H_{j,k} + \zeta_{j,k}^{t-1} - \eta_{j,k}^{t}) + (H_{j,k+1} + \zeta_{j,k+1}^{t-1} - \eta_{j,k+1}^{t}))/2), H_{min}),$$
$$HK2 = MAX(((H_{j,k} + \zeta_{j,k}^{t-1} - \eta_{j,k}^{t}) + (H_{j,k-1} + \zeta_{j,k-1}^{t-1} - \eta_{j,k-1}^{t}))/2), H_{min}),$$
$$SCP = (\cos\varphi_k + \cos\varphi_{k+1})/2,$$
$$SC = (\cos\varphi_k + \cos\varphi_{k-1})/2,$$
$$T - time\ step,$$
$$R\Delta\varphi - north\text{-}south\ grid\ step,\ and$$
$$Rcos\varphi\Delta\lambda - east\text{-}west\ grid\ step.$$

In order to derive a stable solution to the above system, the time step T and space step Δ should satisfy the Courant, Friedrich, and Lewy condition (Ramming and Kowalik, 1980),

$$T \leq \frac{\Delta}{\sqrt{2gH_{max}}} \tag{9}$$

where Δ is the minimum space step and H_{max} is the maximum water depth in the space domain. The term H_{min} is the minimum depth allowable in the computations. This must be fixed to prevent the actual water depth from becoming too small in the bottom friction term and creating an instability.

The ocean boundary conditions are handled as follows. The shoreline is taken along the velocity computation points and the velocity is set to 0 at the boundary which produces pure reflection. The radiation conditions are taken at the open ocean boundaries (Reid and Bodine, 1968).

$$u_{j,k}^{t} = \pm(\zeta_{j,k}^{t-1} * (\frac{g}{H_{j,k}})^{1/2}),\ and$$
$$v_{j,k}^{t} = \pm(\zeta_{j,k}^{t-1} * (\frac{g}{H_{j,k}})^{1/2}). \tag{10}$$

For the west and south boundaries the negative sign is used while for the north and east boundaries the positive sign is applied.

Although the stability condition (9) assures that the time and space steps have been chosen in such a manner that the numerical solution converges toward the analytical solution, the condition does not assure that the numerical solution is close to the analytical solution. In order to achieve an accurate reproduction of a tsunami by the finite difference technique approximately 10 grid points per wavelength are necessary (Ramming and Kowalik, 1980). The long wave phase velocity calculated by a numerical scheme is a measure of the error introduced by numerical approximation. Numerical phase

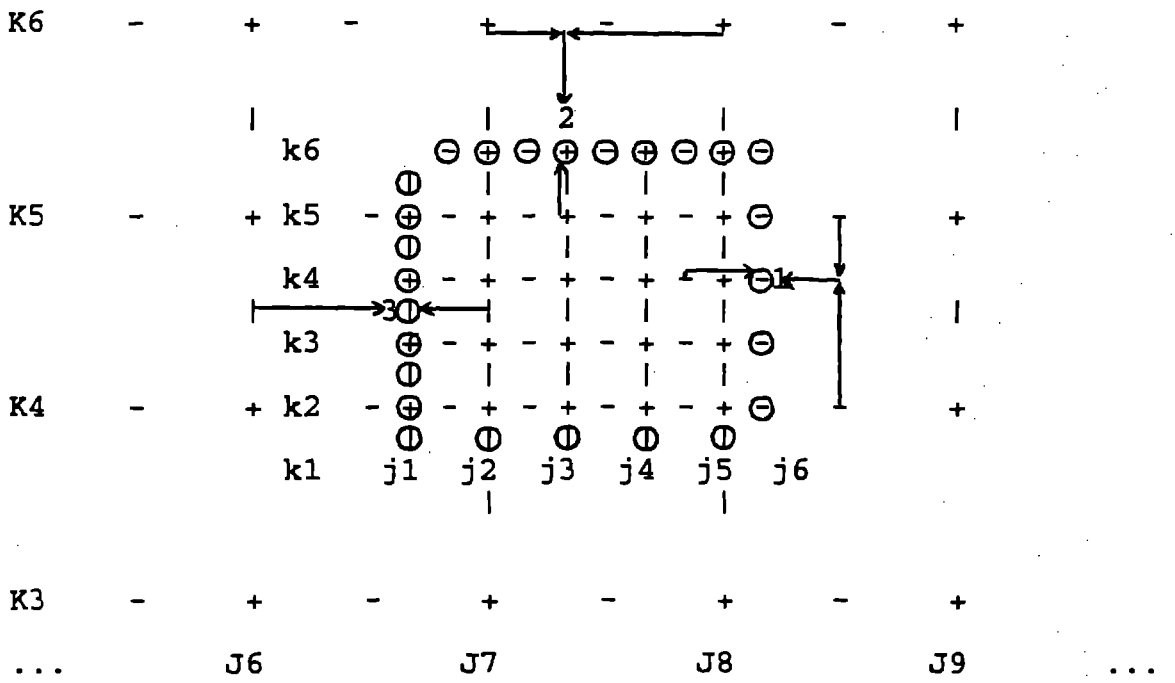

Figure 3. This figure shows the estimations which are performed in the dynamic grid integration scheme used here. Circled sea-levels and velocities represent estimated points used in fine grid calculations. Capital letters are used to denote coarse grid quantities and small letters the fine grid quantities. As an example of how the estimations are made, the points 1, 2, and 3 are computed by

$$u_{j6,k4} = (U_{J9,K5} * 2/FINC + U_{J9,K4} * 1/FINC) * 2/(FINC+1) + u_{j5,k4} * 2/(FINC+1)$$

$$\zeta_{j3,k6} = (\xi_{J7,K6} * 2/FINC + \xi_{J8,K6} * 1/FINC) * 1/FINC + \zeta_{j3,k5} * 2/FINC$$

$$v_{j1,k3} = (V_{J6,K4} * 3/FINC + V_{J6,K5} * 0/FINC) * 1/FINC + v_{j2,k3} * 2/FINC.$$

Here FINC is the increase in resolution from the coarse to fine grid (in this example FINC=3). The velocities on the top and left side of the fine grid are necessary for computing the coriolis and bottom friction forces.

velocity (C_n) depends on the spatial grid distance (Δ) and wavelength (L) (Ramming and Kowalik, 1980)

$$C_n = \sqrt{gH}\left[1-\frac{1}{6}\left(\frac{\pi\Delta}{L}\right)^2\right]. \qquad (11)$$

If we choose the spatial step to be 10 times shorter than the wavelength ($L=10\Delta$), the numerically estimated phase velocity $C_n=0.98(gH)^{1/2}$ will be only 2% smaller than the analytical phase velocity. To demonstrate the error introduced by numerical approximation, we consider a tsunami in a flat-bottom channel. In the left portion of the channel the wave is resolved by 15 grid points per wavelength and in the right portion by only 5 grid points per wavelength. The wave is forced by a sine wave oscillation on the left side and has the open boundary condition given by eq. (10) on the right side. The wave first propagates through the 15 point per wavelength grid, then is dynamically coupled with the 5 point per wavelength grid by the method described below. The sea-level after 12500 seconds is shown in Fig. 2. Note how the fine grid preserves the waveform while in the coarser grid the waveform degrades.

The above consideration implies that as water shoals and wavelength decrease, a finer grid increment must be used to provide at least 10 points per wavelength. Two methods of attaching grids of different spacing are used here. The first is a non-dynamic scheme. Here wave height over time is recorded along a line, or series of lines, in the coarse grid. Next, this wave height output is interpolated and used as input to the finer grid. This method has the disadvantage of no interaction back from the fine grid into the coarse grid. The main advantages to this technique are models that can be run in pieces, therefore using less computer memory, and the time step increment, T, can be optimized for each grid.

The second method of grid splicing used is a dynamic scheme. This scheme solves all grids at each time step which allows the grids to interact with each other. Figure 3 shows graphically how this works. First the u, v, or ζ values are solved over the fine grid, then over the coarse grid. Coarse grid values which overlap the fine grid are then updated with the fine values. Lastly, values around the edge of the fine grid, which are necessary for computations within the fine grid, are linearly interpolated between the coarse and fine grids. This technique can be repeated within the same model for more than just the coarse and fine grid. That is, a 5' grid over the open ocean can be integrated with a 1' grid over the shelf, and this grid integrated with a 12" grid in the bay of interest. The main advantage to this technique is that energy can be transmitted out of the fine grid to interact with approaching waves in the coarse grid. Another advantage of this method is that any space decrease from the coarse to the fine grid, if expressed by an odd whole number integer (3,5,7...), can be handled with the same algorithm. A potential problem is that high frequency waves generated within the fine grid, but not resolved by the resolution of the coarse grid, will be trapped in the fine grid. This can lead to greater-than-expected wave heights in the fine grid.

Source

The main generating force of a tsunami triggered by an earthquake is the uplift or subsidence of the sea-floor which accompanies the earthquake. Determining the actual extent of sea-floor change in a sub-sea earthquake is very difficult. For earthquakes in which no pre- and post-earthquake bathymetry studies have been performed, displacement can be computed from formulae which output surface deformation as a function of fault strike, dip, slip, length, width, depth, moment, and Lame's constants for the surrounding rock (Okada, 1985). These formulae assume an isotropic, homogenous half-space and a simple source configuration. If these assumptions are not true, errors are produced in the resulting displacement field.

Okada's (1985) formulae are used in this study to compute ground displacement from fault parameters provided from detailed seismological studies of the source earthquakes. While these formulae output a static displacement field (i.e., infinite rupture and slip velocity), the static field can be manipulated by the program to simulate a finite rupture velocity. The following studies will test whether a moving source significantly influences the resultant tsunami.

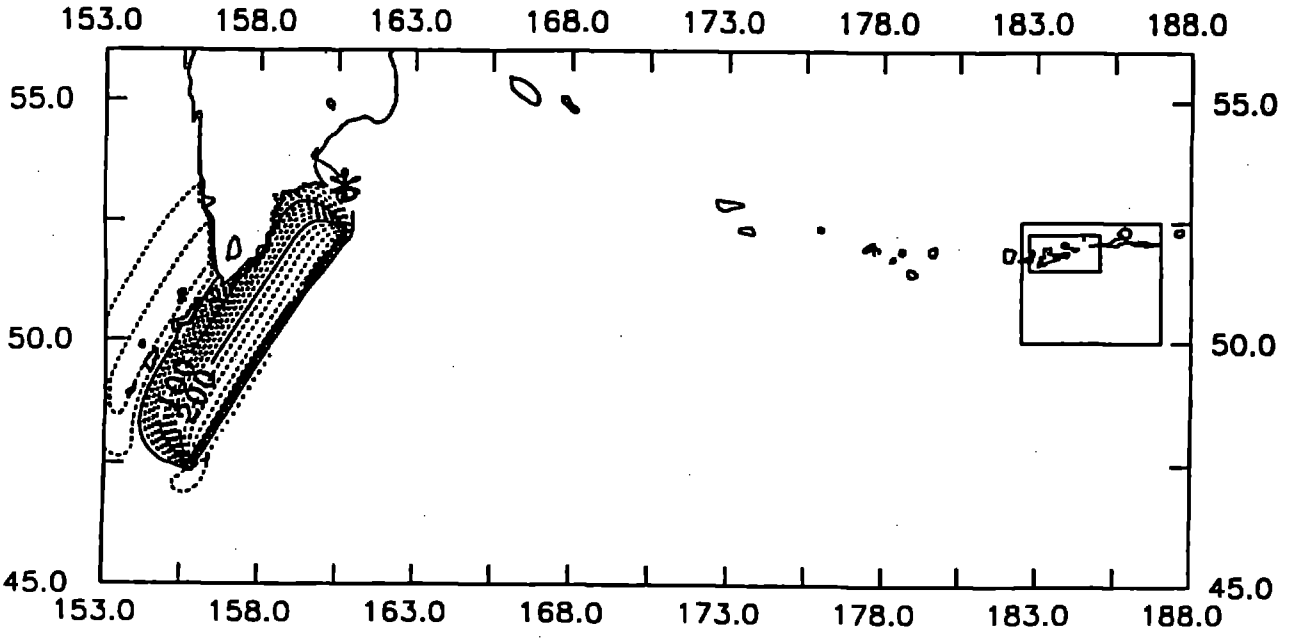

Figure 4. Area modeled with 10' grid. Initial sea-level deviation due to an instantaneous source uplift with fault parameters given in the text for the 1952 earthquake is shown. The sea-level is contoured in cm with an interval of 20cm. The epicenter is marked with an asterisk. The outer box on the right is the area modeled with a 5' grid. The inner box is the area modeled with a 1' grid and shown in Fig. 5. Longitude above 180 relates to west longitude (WLON) by LON = 360-WLON.

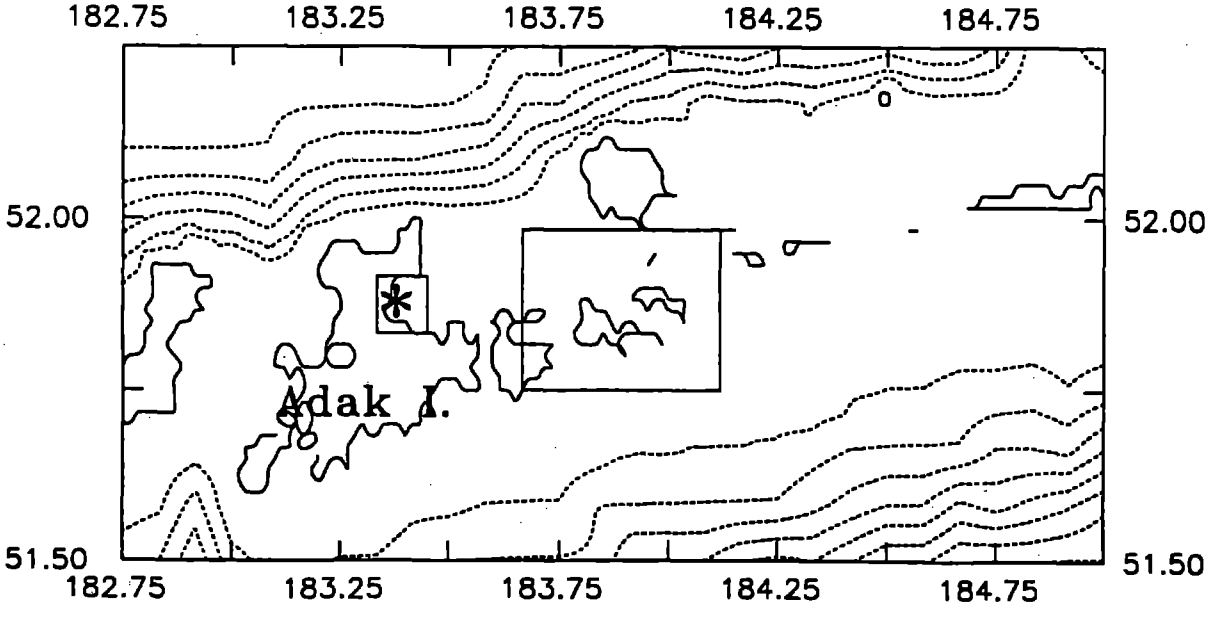

Figure 5. Area which is covered by the 1' grid. Dashed bathymetry contours are in increments of 500m. The asterisk shows where the Adak tide gauge is located. The box around the gauge is the area which is covered by the 12 second grid. The second box east of Adak is also a 12 second grid which defines the inlet channels. Both the 1' grid and the 12 second grid dynamically interact with their respective surrounding grids.

1952 Tsunami Model

An Mw = 9.0 earthquake occurred November 4, 1952 east of the Kamchatka Peninsula. This quake produced a tsunami recorded at tide gauges around the Pacific Ocean. Here the tsunami is modeled over the area shown in Fig. 4 for a comparison with observations at Adak, Alaska.

The earthquake source was studied in detail by Kanamori (1976). Fault parameters are taken from this study and used as input to Okada's (1985) surface deformation equations. Figure 4 displays the initial sea-level configuration due to instantaneous source movement given the fault parameters: length = 650km, width = 200km, depth to bottom of fault plane = 103km, strike = 214°, dip = 30°, slip = 110°, moment = 3.5E29 dyne-cm, and Lame's constants = 4.2E11 dyne/cm^2. The maximum sea-floor uplift produced by this earthquake was 3.3m. Figure 4 shows typical sea-floor movement for subduction zone, thrust earthquakes. That is, uplift on the ocean-side of the trench and broad subsidence toward the back-arc side.

The 1952 tsunami is modeled using a 10′ grid (maximum distance 18.5km) over the area shown in Fig. 4. The sea-level variation over time is recorded at the west and south boundaries of a 5′ grid which extends from 50°N to 52.5°N and from 177.5°W to 173°W. This output is linearly interpolated and used as input to the 5′ grid. The 5′ grid includes a dynamically interacted 1′ grid over the shelf and within that a 12" grid (maximum distance 370m) over eastern Adak Island. The bathymetries within the 1′ grid are displayed in Fig. 5. The 5′ grid and the 1′ and 12" grids within are also used in the next section for modeling the 1986 local tsunami.

The directivity of tsunamis can best be described by the energy distribution radiated from the tsunami source. The maximum energy flux field discussed previously is a better quantity from which to describe directivity then are maximum current or amplitude because it is not water-depth dependent. Figure 6 is a contour map of the maximum energy flux field. The directivity of the energy flux perpendicular to the source is apparent from this map.

As mentioned previously, 10 points per wavelength are needed to accurately propagate a tsunami with the finite difference technique. Table I lists an average number of points per wavelength for the different grid spacings used here assuming the tsunami period is 50 minutes. Modeling indicates the period near the source is less than this, decreasing the number of points per wavelength there.

Table I

grid spacing	depth (m)	wavelength (km)	points/ wavelength
10′ (18.5km)	3000	519	28
5′ (9.25km)	3000	519	56
1′ (1.85km)	150	116	62
12" (0.37km)	60	73	197

Table I indicates that the resolution in this study is more than sufficient to propagate the 1952 tsunami. In fact, we could eliminate the 12" grid and still have enough resolution to model the tsunami. The 12" grid is included to accurately define the area around Adak, to identify the exact location of the tide gauge, and allow us to show how the tsunami amplitude varies at Adak. The 12" grid will also be important in future modeling efforts to include runup effects in the model.

The Coriolis, friction, and non-linear terms in the equations of motion add significantly to the CPU time required to compute a tsunami model. Here, we will test the significance of these terms. Figure 7 shows the modeled tsunami at Adak computed with all terms included in the equations of motion versus the same model with none of the terms included. The cumulative effects of these terms is minor. Each decreases the tsunami amplitude slightly.

Kanamori (1976) modeled the rupture velocity for this earthquake as υ = 3.0 km/s with the fracture propagating unilaterally from NE to SW. The importance of a moving rupture versus instantaneous uplift to the modeled tsunami is tested here. To simulate the propagating rupture the final static displacement is pre-computed. Then, at time steps of 1s, the portion of the fault zone over

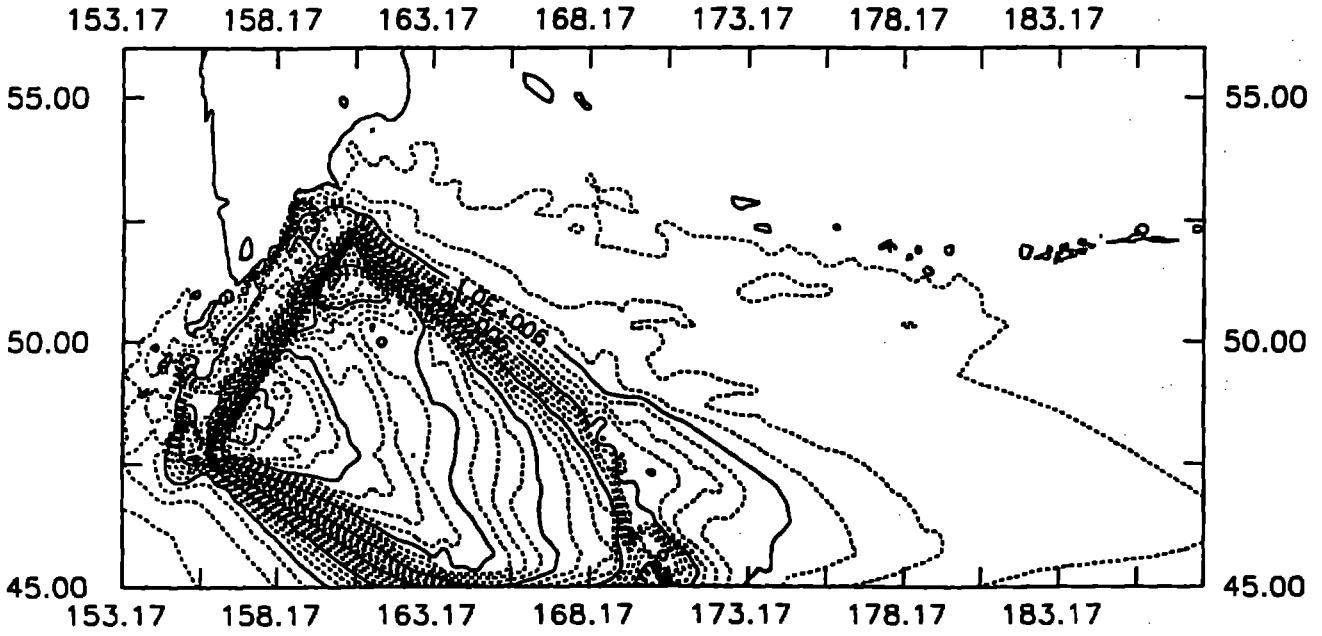

Figure 6. Tsunami energy flux distribution produced by the 1952 Kamchatka earthquake. The source here is instantaneously uplifted. The units are given in Newton/s.

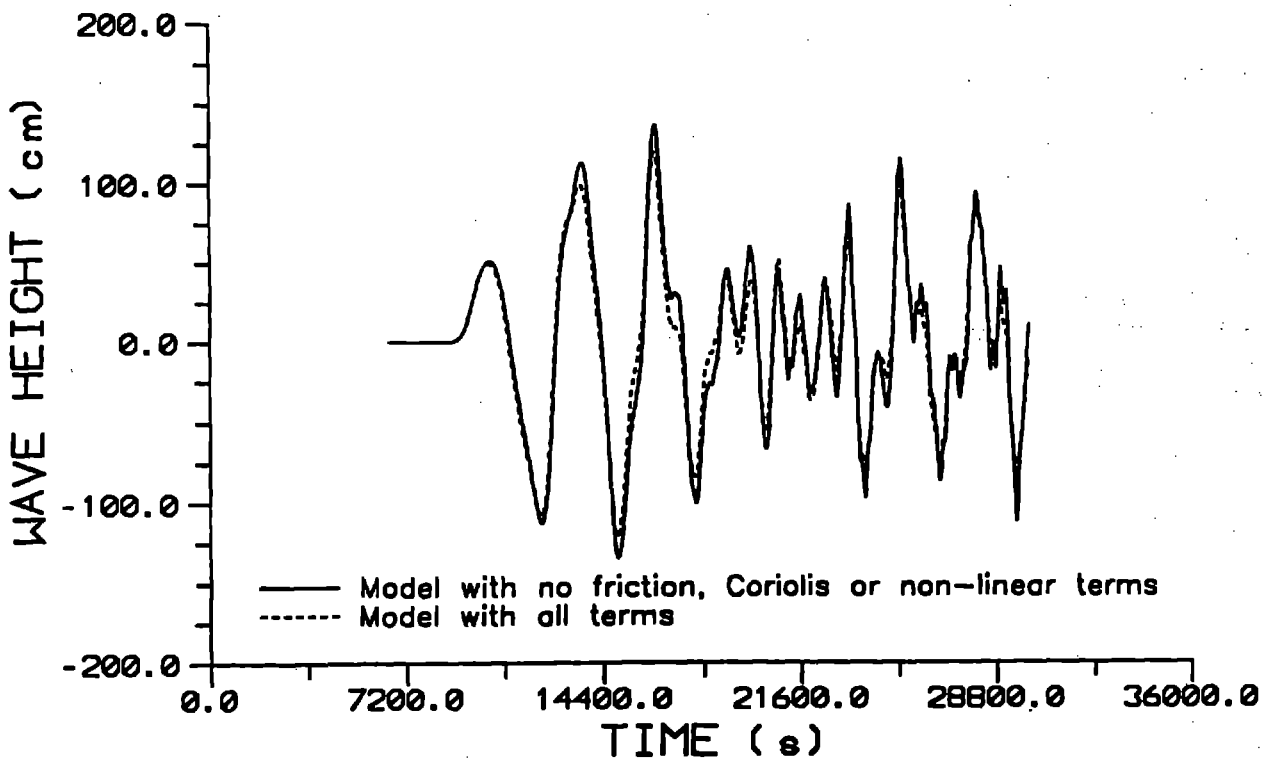

Figure 7. This graph demonstrates the significance of the friction, Coriolis, and non-linear terms in the equations of motion. The combined effect of the three terms in the 1952 tsunami at Adak is to decrease the modeled amplitude slightly. When studied separately each term has a slight negative effect on the modeled amplitude.

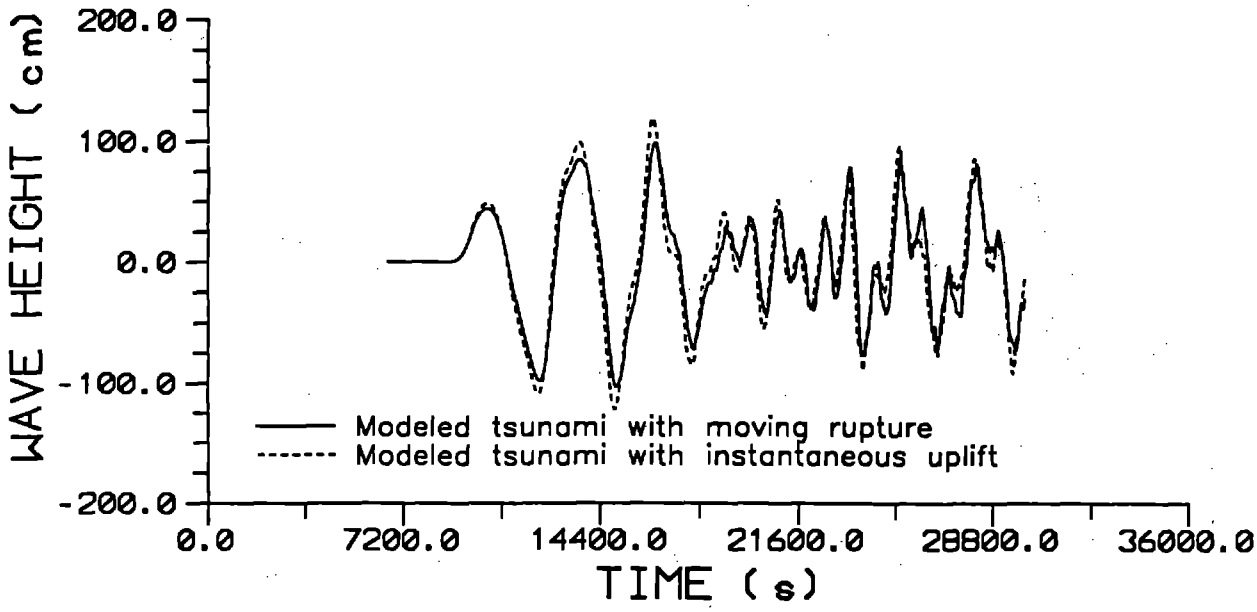

Figure 8. Comparison of instantaneous uplift and moving rupture in the 1952 tsunami modeled at Adak. The moving rupture model shows a decreased amplitude compared to the instantaneous rupture. As explained in the text this decrease is due to the location of Adak with respect to the direction of rupture propagation and the rupture velocity.

which the rupture will have propagated is instantaneously uplifted. For this quake it takes 215s for the rupture to propagate along the entire fault using the average rupture velocity of 3.0 km/s. Figure 8 compares the modeled tsunami with instantaneous uplift versus the tsunami with uplift described above. Both of these models include all terms in the equations. This test shows a decrease in the modeled tsunami amplitude when the source rupture velocity is included.

Marchuk *et al.* (1983) show that for a moving rupture, the tsunami wavefront is directed at the angle $\theta = \pm\arccos(c/v)$ with respect to the direction the fault is propagating. Here, c is the speed of the tsunami. Computing c for the depth = 3000m implies the wavefront is directed at 86.7° from the fault strike versus 90° for an instantaneous uplift. That is, the wavefront is directed more to the south for a moving rupture. Figure 9 demonstrates that the maximum energy flux field is also directed more to the south. This explains the decrease in amplitude at Adak when the moving rupture is simulated.

The comparison of the modeled tsunami to the recorded tsunami at Adak is obtained by including friction, Coriolis, and non-linear terms in the equations of motion with the moving rupture simulated (Fig. 10). This model uses the non-dynamic grid integration scheme for attaching the open ocean grid with the regional model. Within the regional model two dynamic interactions take place. That is, the 5′ to 1′ resolution increase over the shelf and the 1′ to 12″ increase over the area within 10km of the tide gauge.

1986 Tsunami Model

On May 7, 1986 an Mw=8.0 earthquake occurred south of the Andreanof Islands in the Aleutian subduction zone. This earthquake produced a 1.7m tsunami recorded at Adak and was recorded elsewhere in the Pacific Ocean as a small, non-damaging wave. The wave recorded at Adak provides us an opportunity to model a tsunami which was recorded within the source zone. That is, the tide gage at Adak was part of the area of surface deformation produced by the earthquake. A source/receiver configuration such as this is very complicated due to initial waves arriving at the receiver from more than one direction. Several investigators have studied the energy release and fault motion during the Andreanof Islands quake (e.g., Hwang and Kanamori, 1986, Boyd and Nabelek,

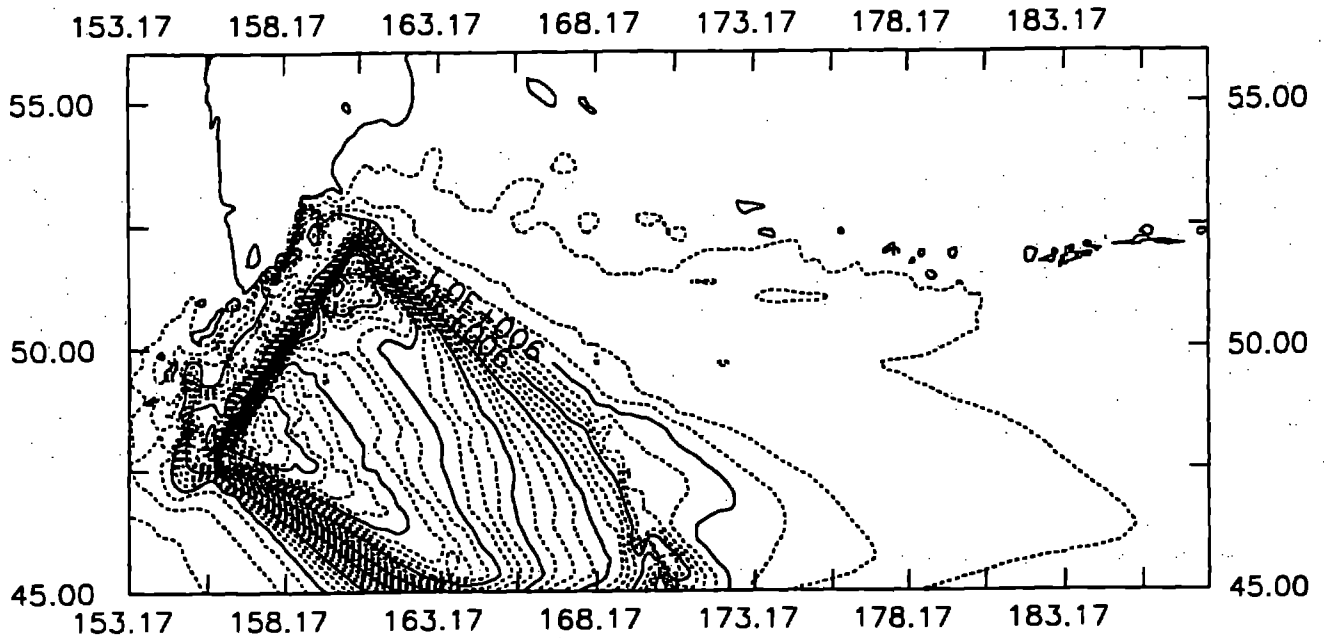

Figure 9. Tsunami energy distribution from the 1952 Kamchatka earthquake. A unilateral rupture (propagating from NE to SW) is modeled here using a rupture velocity of 3.0 km/s. Note there is less energy directed to the north than in Fig. 6. The units are given in Newton/s.

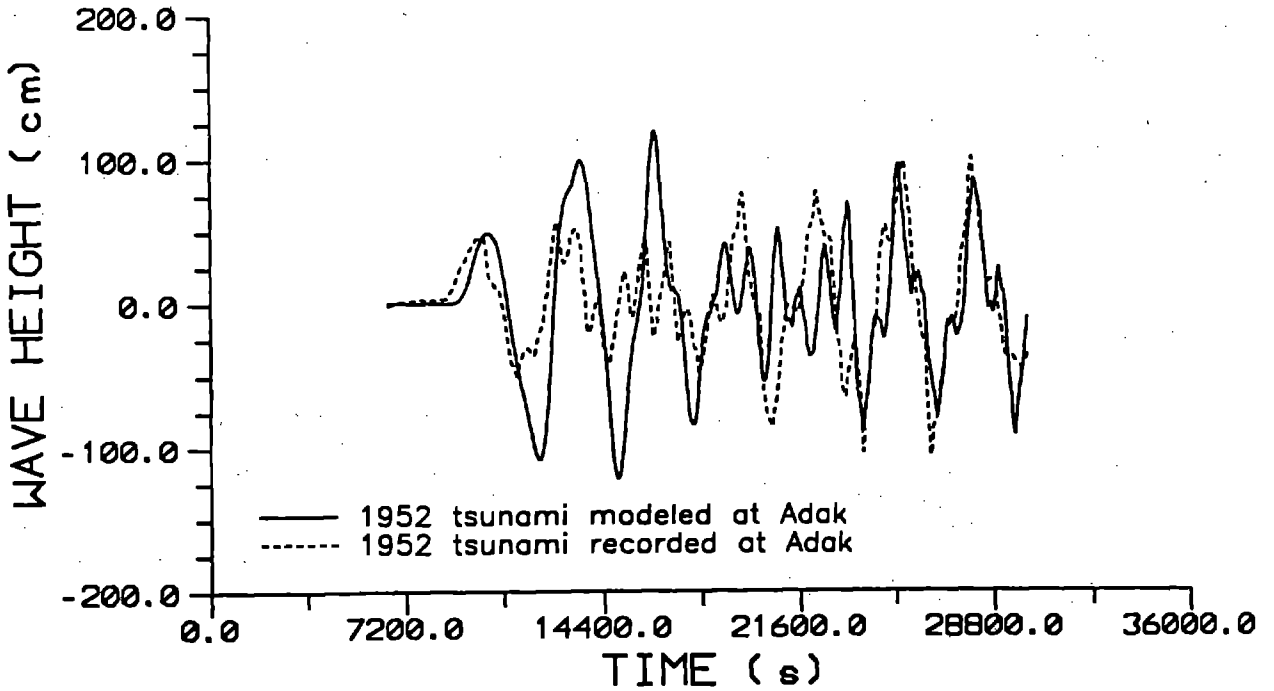

Figure 10. Actual 1952 tsunami recording at Adak shown with the model computed in this study. The modeled tsunami includes friction, Coriolis, and non-linear terms in the equations of motion and accounts for a rupture velocity of 3 km/s. This model was run in two parts (non-dynamically connected) as discussed in the text.

1988, Houston and Engdahl, 1989). Here we use source parameters from Hwang and Kanamori (1986) as input to Okada's (1985) surface deformation equations. Parameters used are: length = 220km, width = 65km, depth to bottom of fault plane = 24km, strike = 257°, dip = 18°, slip = 116°, moment = 1.3E28 dyne-cm, and Lame's constants = 4.2E11 dyne/cm^2. The initial sea-level deviation due to an instantaneous uplift of this source is depicted in Fig. 11. Note that while the main tsunami is generated to the south of the Andreanof Islands, a mild sea-level slope was produced to the north. This slope is a potential wave generating feature.

The finite difference model used to generate and propagate the 1986 tsunami consists of the 5′ grid with the dynamically interacted 1′ and 12" grids as described in the previous section along with a second 12" grid covering the inlet channels east of Adak (Fig. 5). This 12" grid was added to aid in the resolution of these relatively shallow, narrow channels and proved to be helpful in this model as the tsunami has a shorter period than the 1952 tsunami. Table II lists the average number of grid points per wavelength for the different grid spacings used in this model, assuming the tsunami period is 14 minutes.

Table II

grid spacing	depth (m)	wavelength (km)	points/ wavelength
5′ (9.25km)	3000	145	16
1′ (1.85km)	150	33	18
12" (0.37km)	60	21	57

Table II shows that the resolution here should be sufficient to propagate the tsunami from the source to Adak. As an example of the importance of sufficient resolution, Fig. 12 displays the modeled tsunami at Adak using: 1) only the 5′ grid, 2) the 5′ grid dynamically interfaced with the 1′ grid, and 3) the full 5′, 1′, and two 12" grids described above.

Figure 13 compares the observed tsunami at Adak along with the modeled result. The modeled result matches the observed well with respect to wave height and build-up. However, the period in the modeled wave is slightly longer than that in the observed. Marchuk *et al.* (1983) demonstrate that tsunami period is a function of source width. There are several possible explanations of why the source

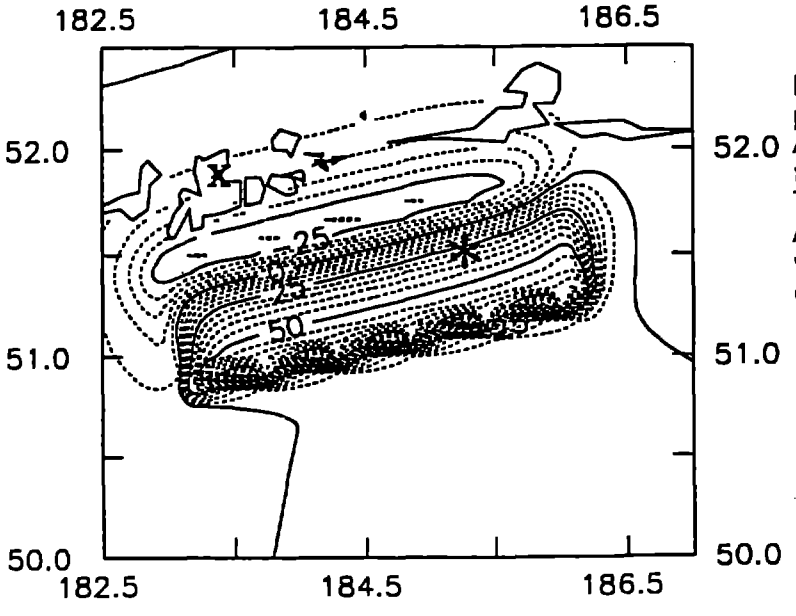

Figure 11. Initial sea-level displacement produced by the 1986 Andreanof Islands earthquake using fault parameters listed in the text. The contour interval is 5cm. The Adak tide gauge location is marked with an 'X' and the epicenter with an asterisk.

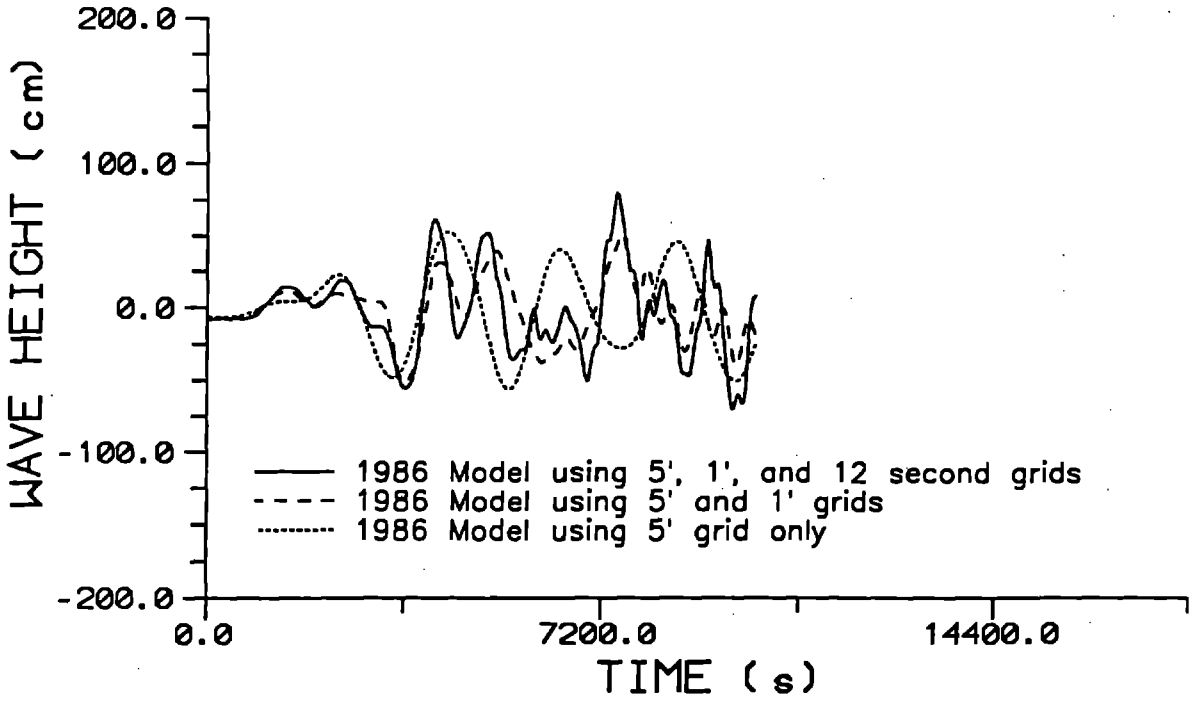

Figure 12. Comparison of the 1986 tsunami model using: Solid – full dynamic integration scheme consisting of 5', 1', and 12 second grids, Dashed – dynamic integration consisting of 5' and 1' grids only, and Dotted – only 5' grid. Note the improved tsunami resolution as finer grids are utilized.

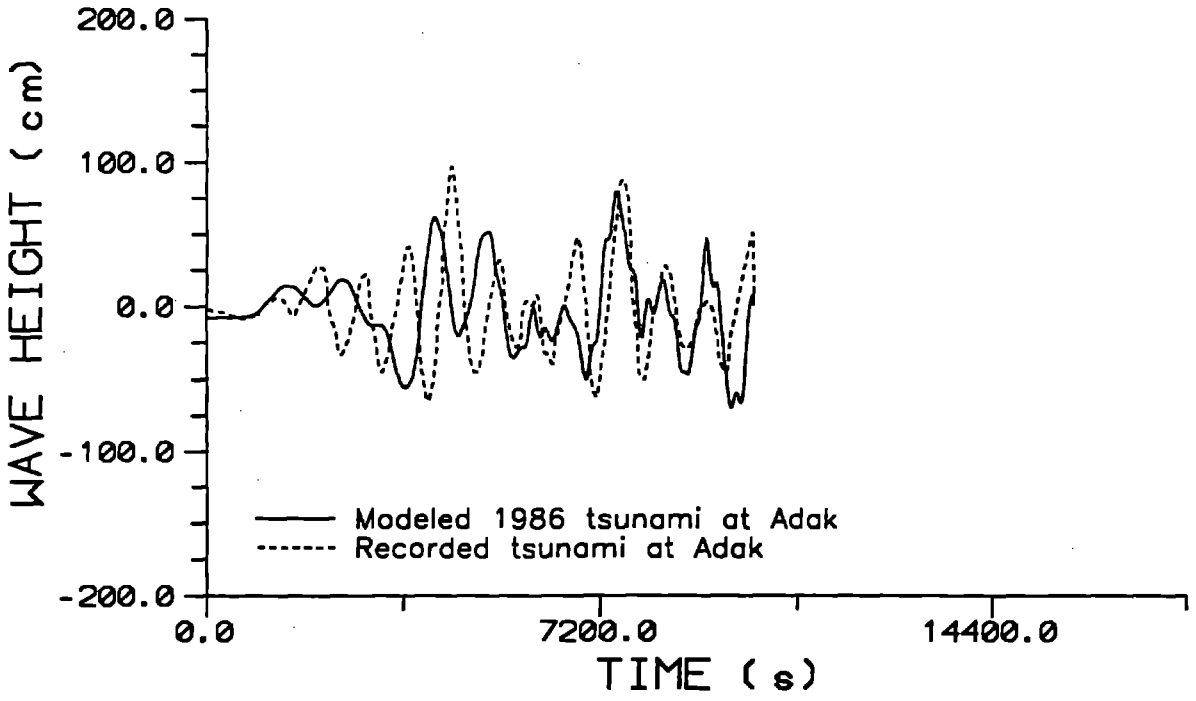

Figure 13. Comparison of modeled and recorded tsunamis at Adak from the 1986 Andreanof Islands earthquake. The modeled result employs friction, Coriolis, and non–linear terms in the equations of motion. The grid used in this model is the 5', 1', and 12 second dynamically interacted grid used for the 1952 model along with a 12 second grid over the inlet channels east of Adak (see Fig. 5).

width computed here is broader than the actual width. First, the fault width taken from Hwang and Kanamori (1986) is greater than the actual rupture width. Second, the surface deformation equations (Okada, 1985), which assume an isotropic, homogeneous half-space, are computing a broader deformation than that which actually occurred. Third, the faulting is more complex than can be accounted for when using the surface deformation equations. Lastly, the effect of waves approaching from more than one direction make the modeled tsunami sensitive to small variations in source configuration.

As was demonstrated in the 1952 model, Fig. 14 shows that the addition of Coriolis, friction, and non-linear terms to the equations of motion make no significant difference in the resultant modeled tsunami. Modeling indicates that the friction and non-linear terms both have a small negative effect on the model which increases with time while the Coriolis force makes no appreciable difference.

Boyd and Nabelek (1988) determined that the average rupture velocity for this quake was 1.5km/s. The earthquake ruptured bilaterally from the epicenter displayed in Fig. 11. Figure 15 compares the tsunami model using an instantaneous rupture velocity with a model using a 1.5km/s rupture velocity. For this earthquake inclusion of finite rupture velocity makes no significant difference in the modeled tsunami.

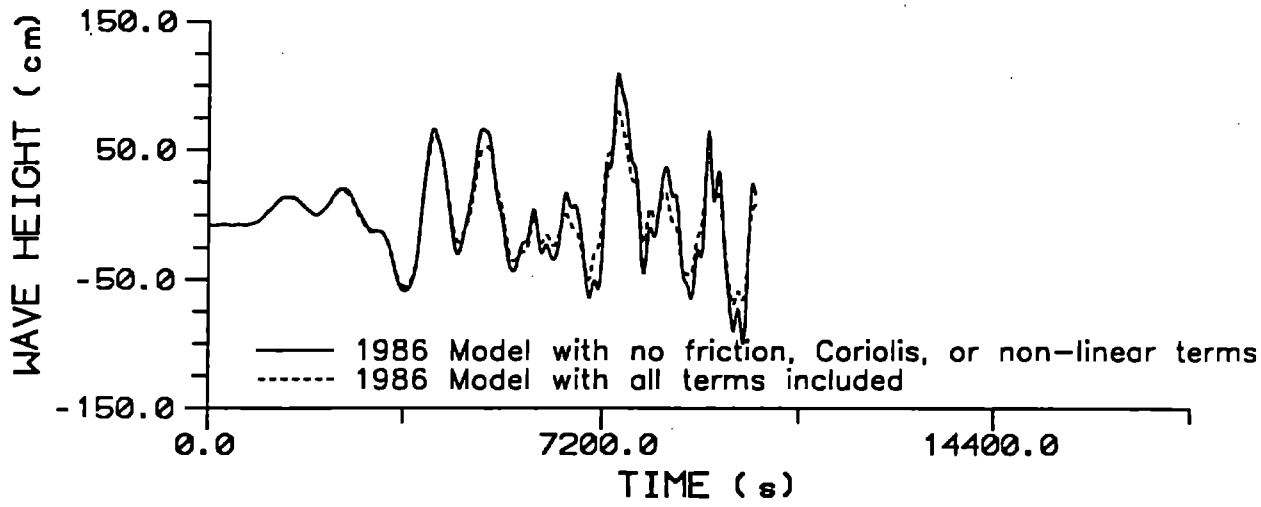

Figure 14. Comparison of the 1986 tsunami model including friction, Coriolis, and non-linear terms in the equations of motion against model without the terms included. The model with all terms included displays slightly decreased amplitude over time.

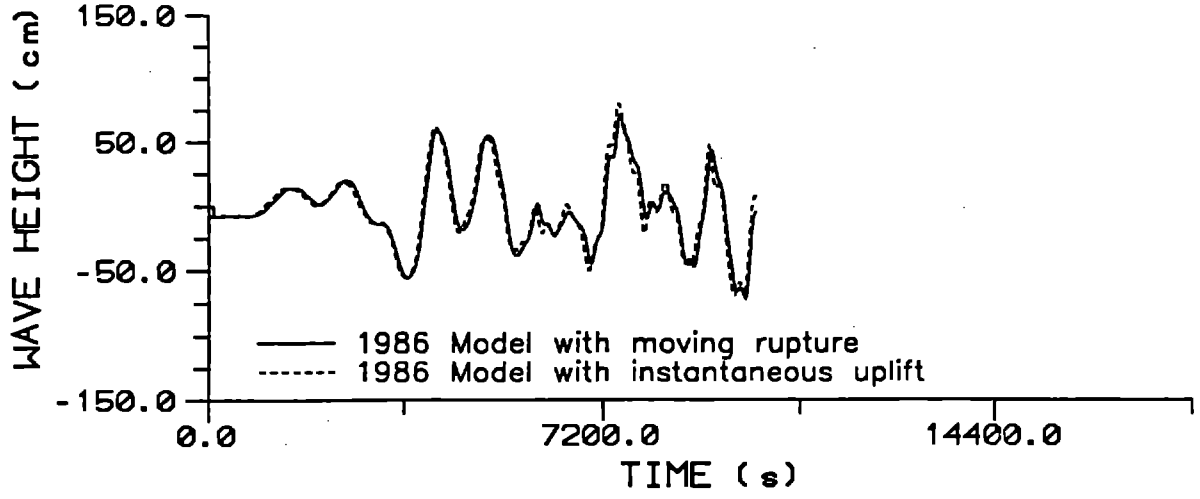

Figure 15. Comparison of the 1986 tsunami modeled using a moving source with a model which used instantaneous uplift but otherwise was identical. The moving source was computed with a rupture velocity of 1.5 km/s (Boyd and Nabelek, 1988). In this model accounting for the moving source makes no practical difference to the modeled tsunami.

Conclusions

Comparisons between observed and modeled tsunamis (Figs. 10 and 13) show that the tsunami modeling technique presented here is successful. The maximum amplitude recorded is within 20% of the modeled amplitude for both tsunamis. We have also shown that the Coriolis, friction, and non-linear terms in the equations of motion can be neglected to save CPU time. Their impact on the modeled tsunamis is relatively minor, though the friction and non-linear terms showed an increasing negative effect with time in the 1986 model. Friction and non-linear terms may show a greater importance in the fine grids when models incorporating runup effects in the very fine grids are employed. The minimum depth allowed, H_{min}, will decrease substantially when runup is accounted for, thus increasing the importance of these two terms. Inclusion of a moving rupture versus instantaneous uplift is also shown to have a small effect on the energy flux distribution and the modeled tsunami. Whether this effect is negative or positive in the modeled tsunami depends on the azimuth of the tide gauge to the rupture vector and on the rupture velocity.

The comparison between recorded and modeled waveforms was better in the 1952 tsunami than for the one in 1986. This is likely due to the tide gauge location within the 1986 source displacement zone. We noted in the many models computed for the 1986 tsunami that a small change in the source configuration could cause a considerable change in the modeled tsunami period and appearance. This may be due to incoming waves from different directions which construct or destruct based on the configuration.

Dynamic connection of grids with different spacing can be accomplished by the method presented here. Spurious effects generated at the boundaries between grids by poor estimations (Ramming and Kowalik, 1980) have not presented a problem in either of the models. These effects are prevented by connecting the grids in water deep enough that the coarser grid sufficiently resolves the wave.

Results from this study have ramifications for community planning at Adak. Figure 16 shows the area near Adak which is covered by a 12" grid (Fig. 5). Both a bathymetric map and an orthographic projection of the maximum amplitude recorded at each grid point in the 1986 model are shown. The maximum amplitude plot shows that the tsunami will attain almost twice the amplitude at the west end of Sweeper Cove compared to the shores just outside the cove.

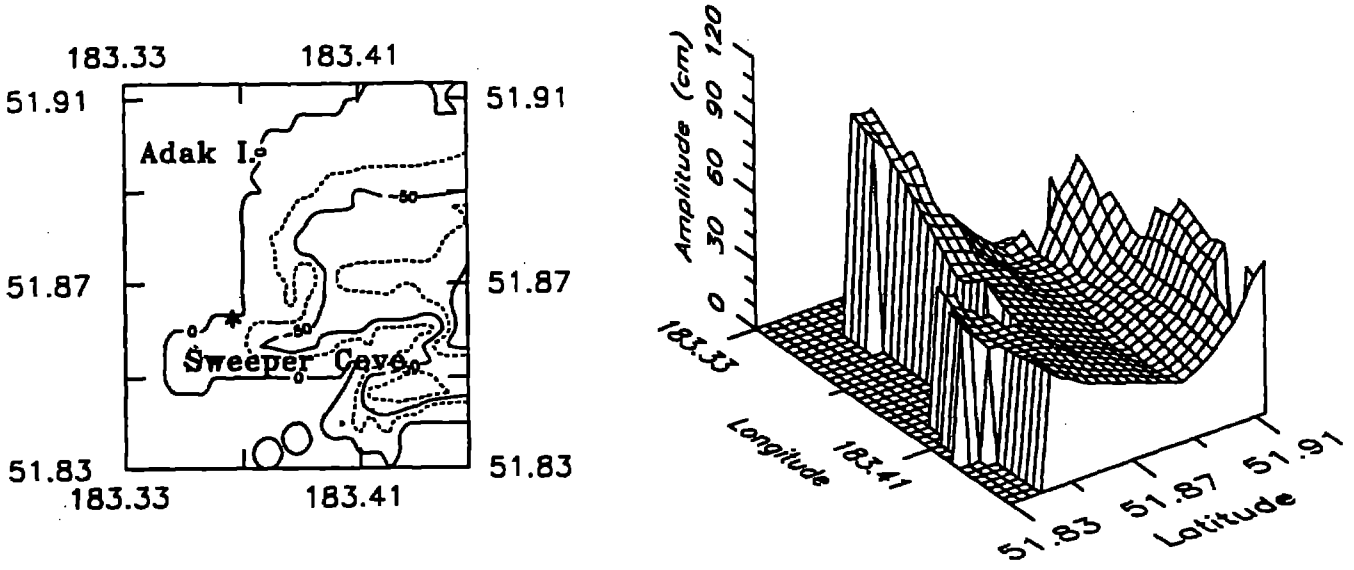

Figure 16. Left display is a bathymetric map of the very fine Adak grid shown in Fig. 5. The contour interval is 25m and the tide gauge location is shown with an asterisk. On the right is an orthographic view of the maximum amplitude recorded at each grid point in the very fine grid in the 1986 model. The view is from the southeast. Note the large increase in amplitude at the west end of Sweeper Cove.

Acknowledgments

The authors wish to express their thanks to Thomas J. Sokolowski, Geophysicist-in-Charge of the Alaska Tsunami Warning Center (ATWC), National Weather Service, for his continued support of this work and the joint tsunami modeling efforts of the University of Alaska, Fairbanks and the ATWC. This study was partly supported by the National Science Foundation Grant BCS 8901122.

References

Boyd, T.M. and J.L. Nabelek, Rupture process of the Andreanof Islands earthquake of May 7, 1986, *Bull. Seism. Soc. Am.*, 78, 1653-1673, 1988.

Gill, A.E., *Atmosphere-Ocean Dynamics*, Academic Press, New York-London, 662 pp., 1982.

Houston, H. and E.R. Engdahl, A comparison of the spatio-temporal distribution of moment release for the 1986 Andreanof Islands earthquake with relocated seismicity, *Geophys. Res. Lett.*, 16, 1421-1424, 1989.

Hwang, L.J. and H. Kanamori, Source parameters of the May 7, 1986 Andreanof Islands earthquake, *Geophys. Res. Lett.*, 13, 1426-1429, 1986.

Kanamori, H., Re-examination of the earth's free oscillations excited by the Kamchatka earthquake of November 4, 1952, *Phys. Earth Plan. Int.*, 11, 216-226, 1976.

Marchuk, A.G., L.B. Chubarov, and I.I. Shokin, *Numerical Modelling of Tsunami Waves* (Eng. trans.), Nauka Press, Siberian Branch, Novosibirsk, 282 pp., 1983.

Murty, T.S., *Storm Surges - Meteorological Ocean Tides*, Bull. 212, Fisheries Res. Board Canada, Ottawa, 897 pp., 1984.

Ng, M., P.H. LeBlond, and T.S. Murty, Numerical simulation of tsunami amplitudes on the coast of British Columbia due to local earthquakes, *Sci. Tsunami Hazards*, 8, 97-127, 1990.

Okada, Y., Surface deformation due to shear and tensile faults in a half-space, *Bull. Seism. Soc. Am.*, 75, 1135-1154, 1985.

Ramming, H.G. and Z. Kowalik, *Numerical Modelling of Marine Hydrodynamics*, Elsevier, New York, 368 pp., 1980.

Reid, R.O. and B.R. Bodine, Numerical model for storm surges in Galveston Bay, *J. Waterway Harbor Div.*, 94(WWI), 33-57, 1968.

Shuto, N., T. Suzuki, K. Hasegawa, and K. Inagaki, Summary of a study of numerical technique on the tsunami propagation and runup, *Proc. Int. Tsunami Symp.*, eds. T.S. Murty and W.J. Rapatz, Inst. Ocean Sci., Sidney, B.C., Canada, 88-92, 1985.

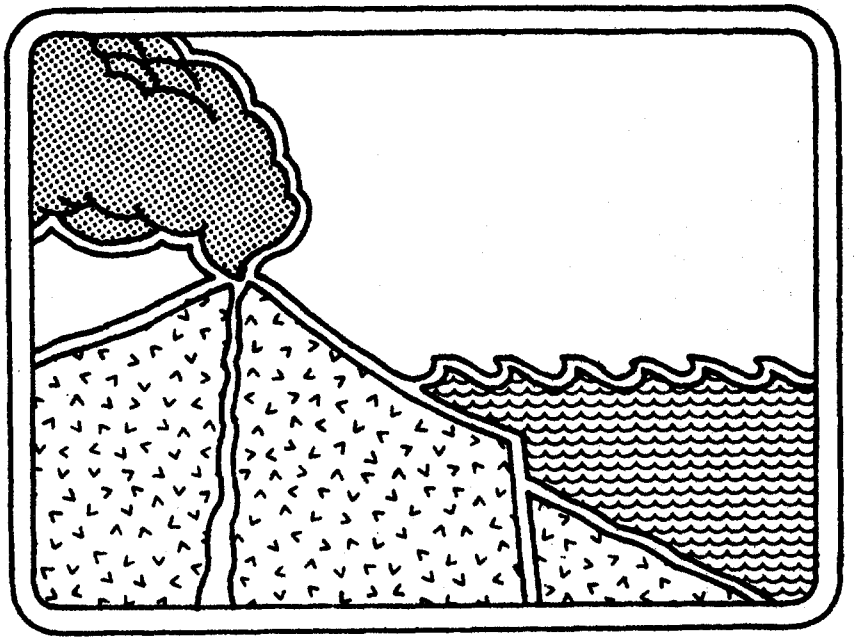

MODELING HILO, HAWAII TSUNAMI INUNDATION

Charles L. Mader
George Curtis
JTRE - JIMAR Tsunami Research Effort
University of Hawaii, Honolulu, HI., U.S.A.

ABSTRACT

The flooding of Hilo, Hawaii by the tsunamis of April 1, 1946, May 23, 1960 and March 28 1964 have been numerically modeled using the non-linear shallow water code *SWAN* including the Coriolis and friction effects. The modeling of each tsunami generation and propagation across the Pacific Ocean to the Hawaiian Island chain was modeled using a 20 minute grid of ocean depths. This furnished a realistic input direction and profile for the modeling of the tsunami interaction with the Hawaiian Islands on a 5 minute grid. The resulting wave profile and direction arriving outside Hilo Bay was used to model the tsunami wave interaction with the bay, harbor and town on a 100 meter grid. Each element of the grid was described by its height above or below sea level and by a DeChezy friction coefficient determined from the nature of the topography.

The 1946 and 1964 tsunamis were generated by earthquakes in Alaska. The 7.5 magnitude 1946 tsunami flooding of Hilo was much greater than the 8.4 magnitude 1964 tsunami. This was reproduced by the numerical model. The directionality of the tsunami from its source was the primary cause for the smaller earthquake resulting in greater flooding of Hilo. The 1960 tsunami was generated by an earthquake in Chile. The observed largest wave was the third bore-like wave. The numerical model reproduced this behavior. The observed levels of flooding for each event was reproduced by the numerical model with the largest differences occuring in the Reeds Bay area where the local topography is poorly described by a 100 meter grid. The observed levels of flooding at individual locations was not well described by the model. Since the front and back of a building at a particular location has been observed to have flooding levels varying by a factor of two, a higher resolution grid including the buildings will be required to describe the flooding at individual locations.

INTRODUCTION

The flooding of Hilo, Hawaii by the tsunamis of 1946, 1960 and 1964 was modeled using the *SWAN* non-linear shallow water code which includes Coriolis and frictional effects. The *SWAN* code is described in Reference 1. Most of the calculations were performed on an IBM PS/2 model 80 with 8 megabytes of memory. The 20 and 5 minute topography was obtained from the NOAA ETOPO 5 minute grid of the earth. The 100 meter grid topography and friction coefficients were obtained using available USGS and other topographic maps, photographs and reports.

The extent of flooding for each event is well documented; however the flooding at individual locations was strongly observer dependent. Often the reported flooding at individual locations varied by a factor of two between the different observers and whether the front or the back of a building was used to evaluate the flooding at a location. The available data sources were collected, and a range of flooding observed for each location determined.

A Hilo tsunami date was selected and the following calculations performed:

First - A 20 minute grid calculation of the North Pacific (and when required for the entire Pacific) was performed to model the tsunami generation and propagation to the region of the Hawaiian Island chain. The 20 minute North Pacific grid was from 120 E to 110 W and 10 N to 65 N and 390 by 165 cells. The wave profile arriving in the region of the chain was used to select a realistic input direction and profile for the second step.

Second - A 5 minute grid calculation of the tsunami wave from the first step interacting with the Hawaiian Island chain was performed. For the 1946 and 1964 tsunami the 5 minute Hawaiian Island grid was from 163 W to 154 W and 18 N to 24 N and 108 by 72 cells. The wave direction and profile arriving in the region of Hilo Bay was used to select a realistic input direction and profile for the third step.

Third - A 100 meter grid calculation of the tsunami wave from the second step interacting with Hilo Bay and Hilo harbor, and the resulting flooding was performed using the input wave direction and profile from the second step. The 100 meter Hilo Bay was 100 by 168 cells and the lower left grid corner was located at 155 degrees, 5 minutes, 40 seconds and 19 degrees, 42 minutes, 45 seconds.

The results of the calculations were compared with the available Hilo flooding levels for each event studied.

TSUNAMI of APRIL 1, 1946

The tsunami of April 1, 1946 was caused by an earthquake of 7.5 magnitude off the Aleutian islands at 53.5 N, 163 W, 12:29 GMT. with a second quake at 12:57 GMT. The source was located about 60 miles SW of Scotch Cap, Unimak Island where the tsunami destroyed the lighthouse and radio towers located more than 30 meters above sea level.

The tsunami arrived at Hilo at about 7:00 a.m. HST with a small crest followed by a large recession. The third wave was the largest. Using the first measurable half-wave period, the period was determined from the Honolulu tide gage to be 15 minutes as described by Green (Ref. 2.) No instrumental record of the tsunami at Hilo was made. The tide at the time of the tsunami was at 20 cm above MLLW and falling.

The earthquake source was estimated by Furamoto (Ref. 3) from the travel times to be 100 km wide and 350 km along the trench. Imaginary wavefronts from observation stations were projected back toward the tsunami source. The presumed source was within the region circumscribed by

the interacting wavefronts. A source with these dimensions was chosen which would result in a large negative initial wave at Hawaii and a run-up of 30 meters near Scotch Cap lighthouse. The source had a sharp dip of 20 meters along the trench on the deep ocean side and decreased linearly to 0 meters along the shallow ocean side of the source. For a 20 minute grid, a cross section consisted of cells of -20.0, -15.0, -10.0 -5.0 meters initial displacement.

The wave arriving north of the Hawaiian Islands was a 1.0 meter high, 1000 second period wave with an initial negative pulse. It arrived from the North with the highest energy directed at the islands. This wave was used as the source for the Hawaiian Island calculation.

The tsunami wave interacted with the Hawaiian Islands and refracted around the island of Hawaii such that the tsunami arrived from the North-East on the Hilo side of the island.

The wave arriving outside Hilo Bay had an initial negative amplitude of 2.0 meters and a 1000 second period, followed by four 1000 second period waves with amplitudes of 3 to 4 meters. This wave was used as the source of the Hilo Bay calculation.

The Hilo Bay calculation was performed for the entire bay for the wave starting from the North and from the North-East. The wave from the North refracted into a North-East wave as it interacted with the bay topography. Both calculations gave similar wave interaction and flooding in Hilo harbor.

The flooding was performed using a constant DeChezy friction coefficient of 30, and using the topography determined DeChezy coefficient array shown in Figure 1. The roughness coefficients for Hilo harbor and town were determined in the Look Lab Hilo Bay model study (Ref. 4). The coefficient of 60 is for open smooth areas, 40 for lava like surfaces, 30 for coral and rougher surfaces, 20 for scattered trees and buildings, 10 for buildings and closely spaced trees.

The calculated and observed inundation limits for Hilo are shown in Figure 2. The calculated and observed inundation limits agree to within the 100 meter grid resolution of the numerical model throughout most of the flooded region.

The calculated and observed flooding levels at various locations in the harbor are listed in Table 1 and shown graphically in Figure 3. The flooding levels are strongly dependent upon the friction. A constant friction model is inadequate to describe either the limits of inundation or the flood levels at individual locations. The numerical model does not exhibit the observed large variability in flooding at different locations. The 100 meter grid is inadequate to resolve local effects of topography or friction that are important at individual locations. The hydraulic model reproduces the observed local flooding levels better than the numerical model. The model values were obtained using the hydraulic model of Hilo at Look Laboratories reported in references 5 and 6.

TSUNAMI of MARCH 28, 1964

The tsunami of March 28, 1964 was caused by an earthquake of 8.4 magnitude in Alaska near Prince William sound at 61 N, 147.5 W, 13:36 GMT.

The tsunami arrived at Hilo at about 17:30 HST with a crest followed by other crests. The second wave was the largest. Using the first measurable half-wave period, the period was determined from the Hilo tide gage to be 50 minutes. A record of the tsunami off Wake island in 800 feet of water was made by Van Dorn (Ref. 7). The wave observed at Wake Island was 15 cm high with a 50 minute period. The tide at the time of the tsunami was at 30 cm above MLLW and rising.

The earthquake source was studied in detail by Plafker (Ref. 8.). The formation of the tsunami

and its interaction (not flooding) with Hilo Bay was modeled by Hwang and Divoky (Ref. 9 and 10). The tsunami was also modeled by Houston, Whalin, Garcia, and Butler (Ref. 11).

The source was 300 km wide and 800 km long aligned along a SW-NE direction. The source was 7 cells wide. The initial amplitudes from ocean to land had heights of +5.0, +9.0, +10.0, +9.0, +5.0, +1.0, -2.0 meters. This source resulted in a wave at Wake Island similar to that observed by Van Dorn (Ref. 7).

The wave arriving north of the Hawaiian Islands was much weaker than for the 1946 tsunami. The wave had a profile of a 0.50 meter high, half-wave with a period of 4000 sec, followed by a 0.1 meter high half-wave with a period of 2000 sec, then by a 0.25 meter high full wave with a period of 1750 sec.

The tsunami wave interacted with the Hawaiian Islands and refracted around the island of Hawaii such that the tsunami arrived from the North-East on the Hilo side of the island. The wave arriving outside Hilo Bay had an initial positive amplitude of 1.0 meters, 4000 second period half-wave, followed by a 1.0 meter 2000 second period half wave, then by a 1.0 meter, 1750 period full wave. This wave was used as the source for the Hilo Bay calculation.

The Hilo Bay calculation was performed for the entire bay for the wave starting from the North and from the North-East. The wave from the North refracted into a North-East wave as it interacted with the bay topography. Both calculations gave similar wave interaction and flooding in Hilo harbor.

The flooding was performed using a constant DeChezy friction coefficient of 30, and using the topography determined DeChezy coefficient array shown in Figure 1.

The calculated and observed inundation limits for Hilo are shown in Figure 4. The calculated and observed inundation limits are much smaller than for the April 1, 1946 tsunami. Throughout most of the flooded region the calculated model gave more inundation than was observed.

The calculated and observed flooding levels at various locations in the harbor are listed in Table 2 and shown graphically in Figure 5. The flooding levels are strongly dependent upon the friction. A constant friction model is inadequate to describe either the limits of inundation or the flood levels at individual locations. The numerical model does not exhibit the observed large variability in flooding at different locations. The 100 meter grid is inadequate to resolve local effects of topography or friction that are important at individual locations. The hydraulic model reproduces the observed local flooding levels better than the numerical model.

The 1946 and 1964 tsunamis were generated by earthquakes in Alaska. The 7.5 magnitude 1946 tsunami flooding of Hilo was much greater than the 8.4 magnitude 1964 tsunami. This was reproduced by the numerical model. The directionality of the tsunami from its source was the primary cause for the smaller earthquake resulting in greater flooding of Hilo. The 1946 tsunami wave peak energy was directed toward Hawaii while the 1964 tsunami wave peak energy was directed east of Hawaii toward the Pacific coast of North America. The large waves observed at Crescent City for the 1964 tsunami and not for the 1946 tsunami are consistent with this directionality difference.

TSUNAMI of MAY 23, 1960

This study required development of a full North and South Pacific grid to determine the nature of the wave arriving at Hilo from South America. A one degree grid from 110 E to 65 W and 65 S to 65 N of 185 by 130 cells and a 20 minute grid of 555 by 390 cells was developed. The one degree grid could only resolve the source with a two cell wide source and gave waves with

periods two times larger than observed. So the 20 minute grid tsunami wave profiles were used to describe the 1964 tsunami.

The tsunami of May 23, 1960 was caused primarily by an earthquake at 19:11 GMT on May 22, 1960 of 8.5 magnitude occurring near Peru, Chile and centered at 38 N and 73.5 W. The major earthquake was preceeded by two 7.5 magnitude quakes at 10:03 and another at 19:10 GMT.

The main tsunami wave crested at Hilo at 12:13 a.m. HST on May 23. The first wave peak was followed by a second peak at 12:46 a.m. then by a third peak (a bore at the harbor entrance) about 20 minutes later which was more than twice as high as the previous waves. This wave was the highest and most destructive tsunami wave in Hilo's history.

The tide at 12:07 a.m. HST was at 60 cm above MLLW and increasing. By the time the largest third and fourth waves arrived the tide was cresting at 70 cm above MLLW.

The earthquake was studied by Plafker and Savage (Ref. 12). The formation of the tsunami and its propagation across the Pacific Ocean toward Hawaii was numerically modeled by Hwang and Divoky (Ref. 9). They concluded that peak wave heights occur along a path roughly normal to the major axis of the elongated source region. They suggested that the preferential directivity may account for the severity of the Chilean tsunami in Japan.

The source was 6 cells or 150 km wide and 21 cells or 800 km long aligned along a N-S direction. The source was six cells wide and an initial upward displacement of 1,2,4,6,4,-2 meters along the width. The waves arrived at the Hawaiian Island chain from the South-East. The wave had a profile of a 0.225 meter high, 3000 second half wave followed by a 0.525 meter high 1500 second wave and then followed by a 0.49 meter high 1500 second wave. The wave that arrived at Johnson Island was similar to the wave reported by Van Dorn (Ref 7).

The 5 minute Hawaiian Island grid was from 170 W to 140 W and 15 N to 25 N and 360 by 120 cells. The tsunami wave interacted with the Hawaiian Islands and refracted such that the wave arrived from the East on the Hilo side of the island. The wave arriving outside Hilo Bay had an initial amplitude of 0.4 meter and a period of 3000 second for 1500 sec, followed by a 1.5 meter 1500 second wave, and then by a 2.0 meter 1500 second wave.

The flooding was performed using a topography determined DeChezy coefficient. The roughness coefficients for Hilo harbor and town were determined by the Look Lab Hilo Bay model study and is shown in Figure 1.

The calculated and observed inundation limits for Hilo are shown in Figure 6. The calculated and observed inundation limits agree to within the 100 meter grid resolution of the numerical model throughout most of the flooded region with the calculated model giving more inundation than observed between Reeds Bay and Pier 2.

The calculated and observed flooding levels at various locations in the harbor are listed in Table 3 and shown graphically in Figure 7. The numerical model does not exhibit the observed large variability in flooding at different locations. The 100 meter grid is inadequate to resolve local effects of topography or friction that are important at individual locations. The hydraulic model reproduces the observed local flooding levels better than the numerical model.

The calculated third wave was largest and steepest in agreement with the observations although the difference in amplitude between the second and third wave is not as large as observed.

The numerical modeling results support the suggestion of Hwang and Divoky that the preferential directivity accounts for the severity of the Chilean tsunami in Hawaii and Japan. The interaction of the tsunami wave with Hilo Bay resulted in modifying the amplitude of the waves from the second being the largest to the third being the largest, steepest and most bore-

like. The wave arriving at Wake Island exhibited none of these characteristics. The interaction of tsunami waves with Hilo Bay is strongly dependent upon their period and their interaction with bay topography and with each other. The relative amplitude and steepness of the waves outside of Hilo Bay may be quite different from the waves flooding the town of Hilo.

CONCLUSIONS

The flooding of Hilo, Hawaii by the tsunamis of April 1, 1946, May 23, 1960 and March 28 1964 have been numerically modeled using the non-linear shallow water code SWAN including the Coriolis and friction effects. The modeling of each tsunami generation and propagation across the Pacific Ocean to the Hawaiian Island chain followed by modeling of the tsunami interaction with the Hawaiian islands on a finer grid and then modeling the tsunami wave interaction with the bay, harbor and town using a high resolution grid results in inundation limits that reproduce the essential features of the actual inundation limits.

The 1946 and 1964 tsunamis were generated by earthquakes in Alaska. The 7.5 magnitude 1946 tsunami flooding of Hilo was much greater than the 8.4 magnitude 1964 tsunami. This was reproduced by the numerical model. The directionality of the tsunami from its source was the primary cause for the smaller earthquake resulting in greater flooding of Hilo. The 1960 tsunami was generated by an earthquake in Chile. The observed largest wave was the third bore-like wave. The numerical model reproduced this behavior. The observed levels of flooding for each event was reproduced by the numerical model with the largest differences occuring in the Reeds Bay area where the local topography is poorly described by a 100 meter grid. The observed levels of flooding at individual locations was not well described by the model. Since the front and back of a building at a particular location has been observed to have flooding levels varying by a factor of two, a higher resolution grid including the buildings will be required to describe the flooding at individual locations.

Acknowledgments

The authors gratefully acknowledge the contributions of Dr. Gus Furamoto, Dr. Harold Loomis, Dr. Lester Spielvogel, Dr. Doak Cox, Dr. Dennis Moore, Dr. Eddie Bernard, Dr. Walter Dudley, Dr. George Carrier, and Dr. Frank Gonzalez. George Nabashima generated the 100 meter grids. The encouragement and support by the members of the Pacific Tsunami Warning Center is also gratefully acknowledged.

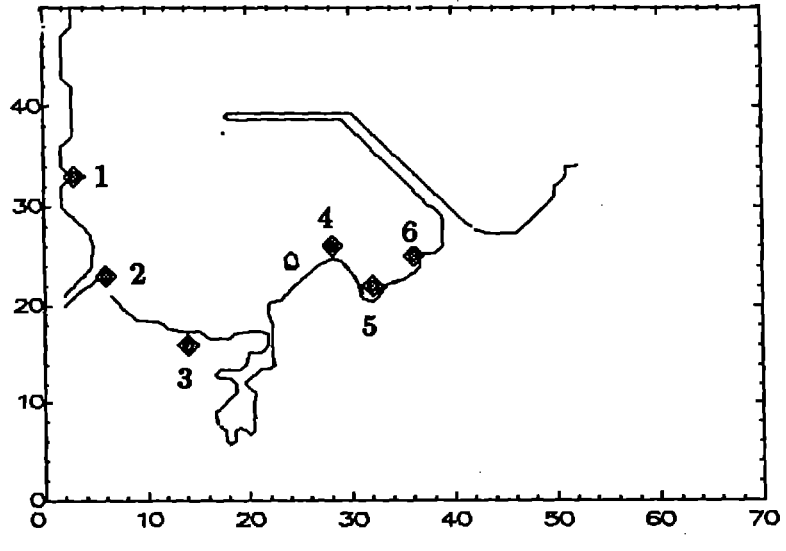

1 Hilo Sugar Mill
2 Wailuku Bridge
3 Theater
4 Waiakea
5 Reeds Bay
6 Pier

TABLE 1

April 1, 1946 Tsunami

Number	Location	Observed	Constant Friction	Topographic Friction	Look Lab Model
1	Hilo Sugar Mill	7.6	9.5	6.2	
2	Wailuku Bridge	7.3-8.5	8.7	5.8	6.1
3	Theater	6.1-8.5	9.0	6.6	
4	Waiakea	6.7-7.9	6.8	4.8	4.2
5	Reeds Bay	2.4-3.0	8.0	5.7	2.4
6	Pier 2	5.8	7.0	6.0	3.4

TABLE 2

March 28, 1964 Tsunami

Number	Location	Observed	Constant Friction	Topographic Friction	Look Lab Model
1	Hilo Sugar Mill		2.8	1.9, 2.0	
2	Wailuku Bridge	1.8	3.0	2.0, 2.1	2.7
3	Theater	0.0	2.9	2.0, 2.0	0.0
4	Waiakea	1.5	3.0	2.5, 3.0	1.8
5	Reeds Bay	2.1	3.0	2.6, 3.5	2.3
6	Pier 2	2.4	3.0	2.5, 3.5	2.1

TABLE 3

May 23, 1960 Tsunami

Number	Location	Observed	Topographic Friction	Look Lab Model
1	Hilo Sugar Mill	4.6-6.1	3.7	6.7
2	Wailuku Bridge	4.3-5.8	4.5	3.8
3	Theater	6.7-8.5	4.5	7.6
4	Waiakea	4.6-6.1	4.2	3.5
5	Reeds Bay	2.7-3.7	4.9	4.1
6	Pier 2	3.6-4.3	5.0	4.4

REFERENCES

1. Charles L. Mader *Numerical Modeling of Water Waves,* University of California Press, Berkeley, California (1988).
2. C. K. Green, "Seismic Sea Wave of April 1, 1946 as Recorded on Tide Gauges," Transactions of 1946 of American Geophysical Union, Vol 27, no 4, 490-502 (1946).
3. A. S. Furamato, private communication (1991).
4. Hilo Harbor Model Conference on 23-24 November 1964 at Look Laboratory of Oceanographic Engineering, Honolulu, HI, Corps of Engineers, U. S. Army Engineer District, Honolulu.
5. "Advanced Information for Participants Hilo Harbor Model Conference on 23-24 November 1964 at Look Laboratory of Oceanography, Honolulu, HI" by U. S. Army Engineering District, Honolulu, HI.
6. "Physically Feasible Means for Protecting Hilo from Tsunamis," Third Report of the Hilo Technical Tsunami Advisory Council to the Board of Supervisors, Hawaii County through its Tsunami Advisory Committee,' December 31, 1965. The committee was Doak C. Cox, Masashi Hom-ma, Masatsugu Suzuki, Ryutaro Takahasi and Robert L. Wiegel.
7. William G. Van Dorn,"Tsunami Response at Wake Island," Journal of Marine Research, Vol 28, no 3, 336-344 (1970).
8. G. Plafker, "Tectonics of the March 27, 1964 Alaska Earthquake" U. S. Geological Survey Professional Paper 543-I, I1-I74 (1969).
9. Li-San Hwang and D. Divoky. "Numerical Investigations of Tsunami Behavior," Tetra Tech, Inc. report (1975).
10. "A Numerical Model of the Major Tsunami," THE GREAT ALASKA EARTHQUAKE OF 1964, National Academy of Sciences (1972).
11. James. R. Houston, Robert W. Whalin, Andrew W. Garcia, H. Lee Butler, "Effect of Source Orientation and Location in the Aleutian Trench on Tsunami Amplitude along the Pacific Coast of the Continental United States" Research Report H-75-4 of U. S. Army Engineering Waterways Experiment Station, Vicksburg, Miss.
12. G. Plafker, and J. C. Savage, "Mechanism of the Chilean Earthquakes of May 21 and 22, 1960", Geological Society of America Bulletin, Vol 81, p 1001-1030 (1970).

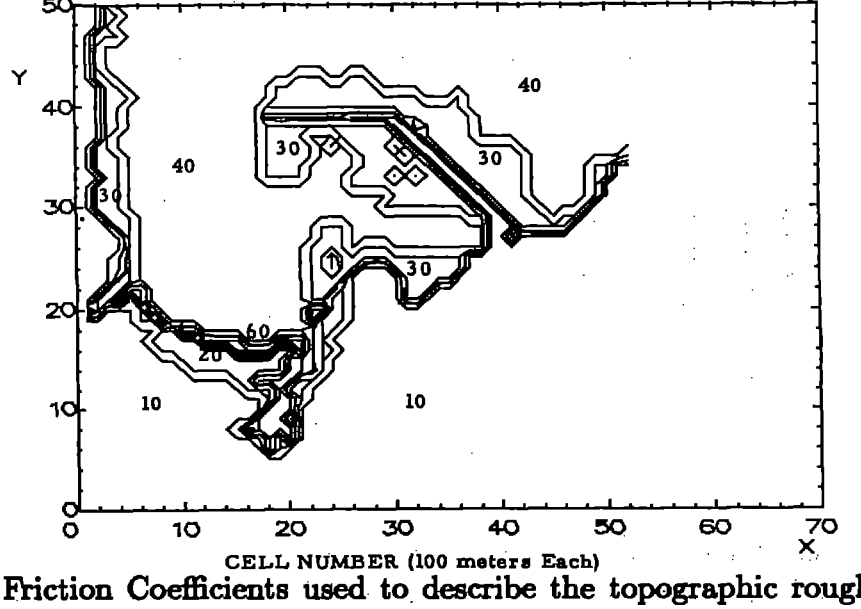

Fig 1. The DeChezy Friction Coefficients used to describe the topographic roughness in Hilo Bay, harbor and town.

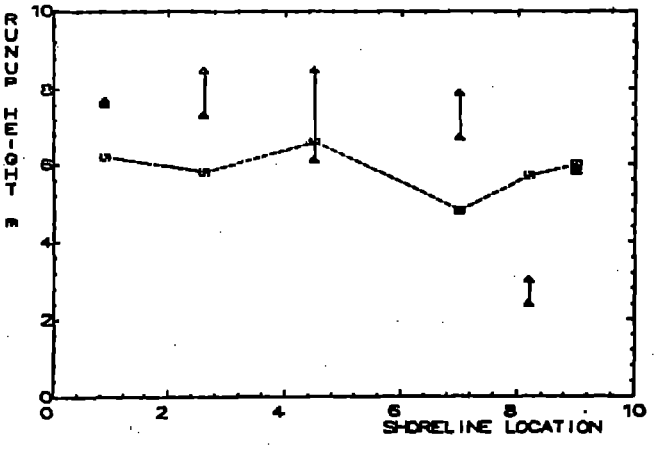

Figure 3. The calculated and observed flooding levels for the April 1, 1946 tsunami at various locations along the shoreline.

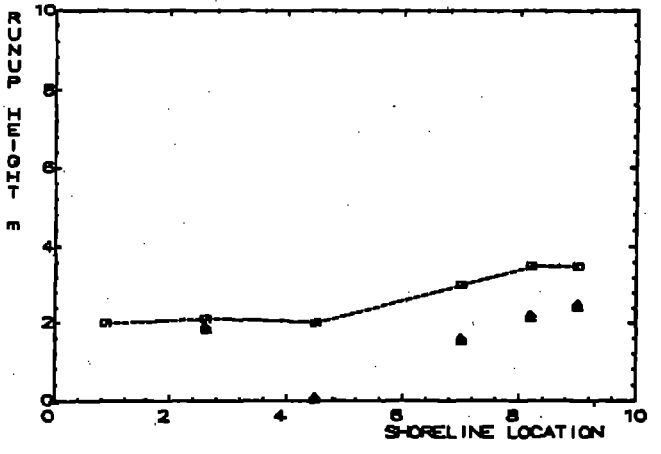

Figure 5. The calculated and observed flooding levels for the March 28, 1964 tsunami at various locations along the shoreline.

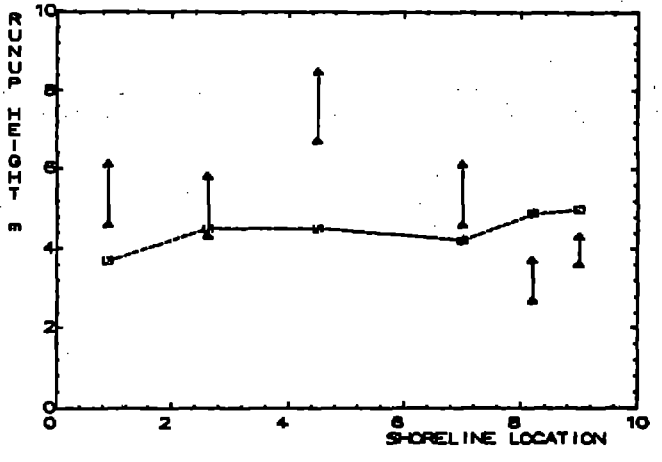

Figure 7. The calculated and observed flooding levels for the May 23, 1960 tsunami at various locations along the shoreline. The locations from left to right are Hilo Sugar Mill, Wailuku Bridge, Theater, Waiakea, Reeds Bay, and Pier 2.

Fig 2. The calculated and observed Hilo inundation limits for the tsunami of April 1, 1946. The observed limit is the heavy dashed line.

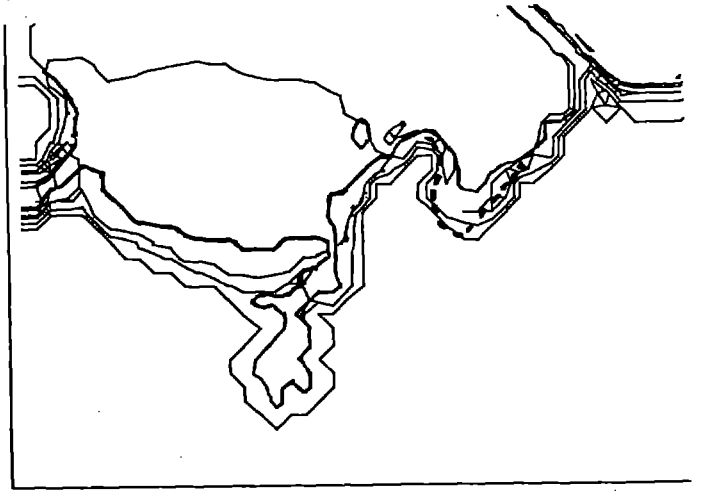

Fig 4. The calculated and observed Hilo inundation limits for the tsunami of March 28, 1964. The observed limit is the heavy dashed line.

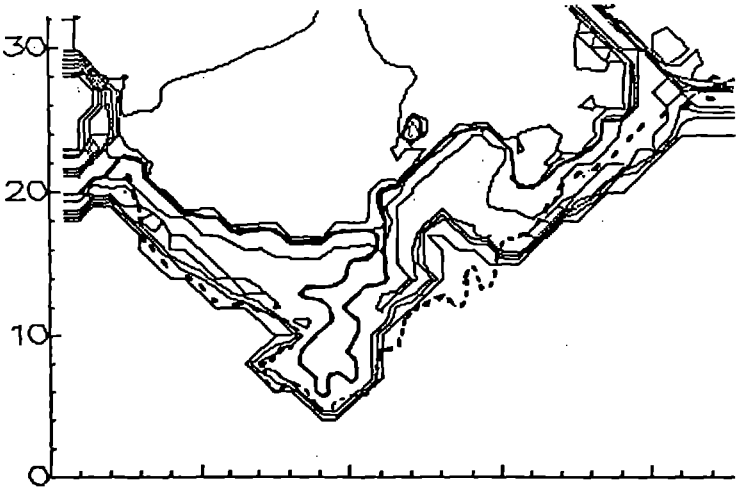

Fig 6. The calculated and observed Hilo inundation limits for the tsunami of May 23, 1960. The observed limit is the heavy dashed line.

SOURCE PARAMETERS OF DESTRUCTIVE TSUNAMIS

Augustine S. Furumoto
Hawaii Institute of Geophysics
School of Ocean and Earth Science and Technology
University of Hawaii, Honolulu, Hawaii, U. S. A.

ABSTRACT

Published lists of tsunamis were combed to find destructive transoceanic tsunamis from 1800 to 1990. Fifteen tsunamis were so identified. The common factor in this class of tsunamis was the frequent occurrence of runup heights equal to or greater than 4 m at distances greater than 1000 km from the source.

These tsunamis were divided into major and giant tsunamis according to size. In cases where moment magnitudes or their equivalents were obtainable, earthquakes that generated giant tsunamis had moment magnitudes equal to or greater than 9 and rupture lengths longer than 550 km. Generators of major tsunamis had moment magnitudes from 8.4 to 8.8 and rupture lengths from 240 km to 530 km. Generators of locally destructive tsunamis were also examined and it was found that these generators had moment magnitudes less than 8.2 and rupture lengths less than 280 km. These values however do not constitute rigid criteria because determinations of magnitudes have errors of ± 0.25 and rupture lengths can be in error of 100 km.

Implications for tsunami response plans are discussed and it is suggested that response plans be tailored to the size of tsunamis.

INTRODUCTION

Within the Pacific Ocean Basin and along its marginal seas, tsunamis are generated frequently by earthquakes. In the tabulation of destructive earthquakes of the world compiled by Utsu [1] are listed 372 occurrences of tsunamis in the Pacific Region from January 1800 to December 31, 1989, on the average of two tsunamis per year. Tsunamis come in different categories: (1) most cause no damage; (2) some cause severe damage in the meizoseismal area and then travel across the ocean but cause no damage to distant shores; and (3) a small number after causing havoc in the meizoseismal area travel across the ocean thousands of kilometers to inflict death and destruction to distant coastal communities. Corresponding to the above criteria for the purpose of this paper tsunamis are classified into (1) no-damage tsunamis; (2) destructive local tsunamis; and (3) destructive transoceanic tsunamis. As will be shown later in this paper, the third class of destructive transoceanic tsunamis can be further subdivided according to size into major and giant types.

This paper intends to contribute toward the formulation of appropriate response plans for destructive transoceanic tsunamis. Thanks to the efforts of the staff of the Pacific Tsunami Warning Center located in Ewa Beach, Hawaii, usually there is a time interval of hours between the issuance of a tsunami warning by the Center and the arrival of a tsunami at distant shores. Upon reception of a tsunami warning, there is ample time for each local political entity, whether a nation, state, province or municipality, to mobilize its resources according to its respective response plan. However most response plans are based on worst case scenarios and consist of evacuation of perceived potential inundation areas. If industrial and commercial enterprises are located in the potential inundation areas, mandatory evacuation results in suspension of vital economic activities. Because the response plans were based on worst case scenarios, when the tsunami finally arrives, usually only a fraction of the evacuated area is inundated. Then the authorities who had put the response plan into operation had to sustain criticisms of over-reaction. Because tsunamis come in different sizes, there should be flexible response plans to meet the different sizes of tsunamis. We attempt to identify the parameters that will enable emergency management administrators to judge the size of an approaching tsunami so that more appropriate response plans can be selected in real time during a tsunami alert or warning.

If flexible response plans are to be adopted, the first step is to discriminate between destructive local tsunamis and destructive transoceanic tsunamis. The Pacific Tsunami Warning Center may have to issue a tsunami warning even in the case of a destructive local tsunami because its responsibility is to the entire Pacific Basin community of nations. The emergency management agency at the local level should discriminate between local and transoceanic tsunamis before selecting the appropriate response plan. We address the question of how to discriminate between destructive local and transoceanic tsunamis.

We have examined the historical records of tsunamis and found that of the 372 tsunamis in the Pacific Ocean and marginal seas between 1800 and 1990, there were 15 events that can be classified as destructive transoceanic tsunamis. Of these, 8 were of such severity that the worst case scenario type response plans would have been appropriate, and we call these giant tsunamis. For the other 7, worst case response plans would have been an over-reaction and an unjustifiable drain on the economy of the communities affected. The second class will be referred to as major tsunamis. We also address the question of how to distinguish a major tsunami from a giant tsunami.

LIST OF DESTRUCTIVE TRANSOCEANIC TSUNAMIS

The databases we searched to find destructive transoceanic tsunamis were bound volumes of tsunami data [1], [2], [3], [4], [5], [6], as well as journal articles [7], [8].

Diurnal tidal variation can affect tsunami inundation. The parameter called runup height used in the catalog by Iida et al. [2] considers the effect of tides. Fortunately this parameter has been adopted by the other catalogs listed in the previous paragraph so that there is a uniform parameter to quantify tsunami inundation.

Shepard et al. [7] classified tsunamis that invaded the shores of Hawaii as having caused "severe," "moderate," "small" or "none" damage. This information aided us in classifying tsunamis according to size. When runup heights as given in other sources were correlated with the adjectives used by Shepard et al., it was found that "severe" and "moderate" tsunamis had runup heights of about 4 m or greater in many places in Hawaii. Hence we used 4-m runup height as our criterion for selection.

Of the "severe" tsunamis listed by Shepard et al. [7], we decided not to consider that generated by the Great Kau Earthquake of April 2, 1868, because, although it raised havoc in the meizoseismal area on the southeast coast of the island of Hawaii, it was reduced to a height of 1.5 m at Honolulu Harbor, a distance of 300 km from the earthquake epicenter. This was a "severe" local tsunami.

For our selection we chose tsunamis that caused runup heights of 4 m or more at distant shores, 1000 km from the earthquake epicenter. We found that 15 events fell into our category of destructive transoceanic tsunamis (Table 1). The table includes the range of runup heights at different distant shores and the tsunami magnitude as calculated by the compilers of tsunami data.

The information and data listed in Table 1 may need a few words of explanation. For example, questions may be asked as to why there is a question mark associated with the source location of the tsunami of 1869. On July 24, 1869 tsunami arrivals were observed all over the Hawaiian Islands. Later examinations of earthquake records around the Pacific Ocean failed to uncover any earthquake that could have generated the tsunami. The waves were not storm surges, as Hawaiians were well experienced in distinguishing between tsunamis and storm surges. The several reports of tsunami heights higher than 4 m in the Hawaiian Islands and the resulting "moderate" damage qualified this tsunami to be classified as destructive transoceanic. However, there has been no tsunami damage reported from outside the Hawaiian Islands for this date. Shepard et al. [7] have suggested the source to be South America whereas Lander and Lockridge [5] have suggested the South Pacific.

The tsunami generated by the Sanriku, Japan, earthquake of June 15, 1896 requires some justification to be included with other destructive transoceanic tsunamis. Shepard et al. [7] has listed the tsunami as having caused "none" damage, but examination of other databases showed that the runup heights ranged from 3 m to 5.5 m along the Kona Coast, the western coast of the island of Hawaii. The judgment of "none" damage is correct for the nineteenth century because the Kona Coast was a sparsely populated rural district where the inhabitants lived by taro farming and fishing. Although in 1896 the tsunami inundated many places, no damage was done to the houses along the coast, as the inhabitants, heeding centuries of experience, had constructed their modest homes in places safe from tsunami inundation. On the other hand, should there be a repeat of the tsunami of 1896, damage will be widespread along the Kona Coast which is now a highly developed resort area. There will be a high price to pay for restoration of life lines such as roads, highways and utilities, and the hotels built close to the seashore will suffer from salt

water soaking.

The Hawaiian Islands are situated in an advantageous position for classification of tsunamis. Centrally located in the Pacific Ocean, they are in the path of tsunamis from around the Pacific Rim, and as diurnal tidal variation in the Hawaiian Islands is about 0.6 m [5], variation of tsunami damage by tidal difference is insignificant. How widespread damage is by tsunami in the Hawaiian Islands can be used to judge the size of a tsunami. We shall designate as "giant" those tsunamis that have done damage throughout the Hawaiian Islands and as "major" those that have done damage in selected places. For example, the tsunami of April 1, 1946 will be considered giant because it caused death and destruction throughout the Hawaiian Islands, whereas the tsunami of 1896 will be regarded as major because its potential for damage was limited to the Kona Coast of the island of Hawaii. When so classified, there were 8 giant tsunamis and 7 major ones.

Although our classification resulted from consulting damage and runup height reports from throughout the Hawaiian Islands, in Table 1 the giant tsunamis correspond with "severe" damage and major tsunamis correspond with "moderate" damage or less. It should be reminded that in Table 1 we have deleted local destructive tsunamis, although the local tsunami of 1868 caused "severe" damage.

SOURCE PARAMETERS OF DESTRUCTIVE TRANSOCEANIC TSUNAMIS

For the tsunamigenic earthquakes listed in Table 1, we gathered the following source parameters from published literature: (1) depth of earthquake focus, (2) surface wave magnitude, M_s; (3) seismic moment, M_o; (4) moment magnitude, M_w; (5) earthquake magnitude by tsunami data, M_i; and (6) sizes of source areas. The collated information is listed in Table 2. We did not list the seismic moments in the table since the moment magnitudes, M_w, were derived from the seismic moments, Mo, by use of the textbook formula [10]:

$$M_w = .67(\log M_o) - 10.7. \qquad (1)$$

The fifth and sixth parameters, magnitude by tsunami data and sizes of source areas, need explanation. As determination of seismic moment requires records from long period seismographs, Abe [9] devised a method to determine magnitude from tsunami data for those earthquakes that do not have long period records. By appropriate normalization, he has shown that the magnitude by tsunami data can be made numerically equivalent to moment magnitude. Hence in Table 2, magnitude by tsunami data can be considered to be equivalent to moment magnitude. Moment magnitudes for some earthquakes earlier than 1960 were obtained in a round about way by considering the size of the meizoseismal area [9]. It should be clarified that earthquake magnitude by tsunami data M_i is an index of the energy content of the earthquake whereas tsunami magnitude m is the index of the size of the water wave in a tsunami.

Tsunami source areas can be calculated in several different ways. The basic assumption is that the tsunami source area coincides with the rupture area of the generating earthquake. Rupture areas can be derived from any one of following methods: (1) plotting the aftershock area; (2) inversion of long period body waves; (3) inversion of surface wave data; and (4) inversion of tsunami data. Of these, the most direct method for tsunami source delineation is the inversion of tsunami data, but this method has been the least used of the four methods. The first

method, plotting of aftershocks, is based on the assumption that the aftershock area coincides with the rupture area of an earthquake. This has been a widely accepted assumption among seismologists although a definitive demonstration of the validity of the assertion has so far eluded publication. Aftershock method is the most indirect of the four methods, but it has been the most widely used.

The Aleutian earthquake and tsunami of April 1, 1946 have been a mystery to seismologists, therefore we shall devote a section to the problem related to the tsunami source area.

Aleutian Earthquake and Tsunami of April 1, 1946.

Of all the tsunamis listed in Table 1, the Aleutian tsunami of April 1, 1946, caused the most wide-ranging devastation. In Hawaii it has been the most destructive tsunami in terms of deaths and damage since recorded history began and in the Marquesas Islands recorded run-up heights amounted to 9 to 10 m. Yet, the surface wave magnitude M_s of the generating earthquake calculated from seismograms was only 7.4. Sykes' [11] plot of the aftershocks gave an elliptical area 170 km by 100 km, a rather small area for such a destructive tsunami. Because of the low quality of seismograms during that time, only eight months after the end of World War II which had left many seismograph stations understaffed and in need of extensive repairs, records usable for seismic moment calculations are not available in the archives. However, Abe [9] determined the earthquake magnitude by tsunami data M_t as 9.3.

Hatori [12] attempted to determine the tsunami source area by using tsunami data and outlined a source length of 400 km and an area of 48,000 sq km. To determine the western end of the source area, he retraced the tsunami arriving at Miyako and Ayukawa in Japan to its source, but for the eastern anchor he assumed that the aftershock area given by Sykes [11] was appropriate.

We decided to redetermine the tsunami source area by retracing the waves to the source. For the western edge of the generating area, we agreed with Hatori and accepted his determination. But we disagreed on the appropriateness of using the aftershock area of Sykes for the eastern end. We examined the tide gage records of the tsunami as published by Bodle [13] and Green [14] and picked the tsunami arrivals for Yakutat, Sitka, Crescent City, La Jolla and Valparaiso, and then used the Tsunami Travel-Time Charts published by the U. S. Department of Commerce, National Oceanic and Atmospheric Administration (1971), to retrace the tsunami to its origin time. The selection of tide gage records was limited by the availability of travel time charts. The tide gage records of Sitka and Yakutat (Fig 1) illustrate where we had picked the tsunami arrivals. At Sitka the first upward motion of a 20-minute wave was selected as the arrival; at Yakutat the beginning of a 30-minute period, somewhat obscured by background oscillations, was selected as the arrival. Tide gages from Crescent City, La Jolla and Valparaiso had such definitive first arrivals that there was no doubt about when the tsunami arrived. In Table 3 are the arrival and travel times of the tsunami to the five stations. The results of retracing the tsunami to its origin time are shown in Figure 2. The elliptical area which we consider to be the tsunami source area is 570 km x 260 km, an area of roughly 150,000 sq km. This is a respectable generating area.

The discrepancy between the severity of this tsunami and the apparent low energy release of the earthquake as indicated by surface wave magnitude rests with the poor quality of seismological observation in the early months of 1946. World War II had only ended eight months prior to the earthquake and the seismograph stations were in need of staff members and

repair. Besides the problem of maintenance, seismographic data of those days were not suited for seismic moment calculation. Furthermore, epicenter determinations were done in the tedious and time consuming graphic method on a model globe. The list of epicenters of the aftershocks published by the United States Coast and Geodetic Survey for this earthquake show that about half of the aftershocks have the same geographical coordinates as the main shock. This is not consonant with aftershock distributions of similar large earthquakes.

The curious phenomena associated with the earthquake and tsunami of April 1, 1946 do not constitute a puzzle. It was just unfortunate that such a giant tsunami should have been generated at a time when seismological observation was at the lowest ebb since the invention of the seismograph.

Source Parameters of Giant and Major Tsunamis.

When comparing Tables 1 and 2, we note that all the tsunamis that were classified as "severe" in the Hawaiian Islands had magnitudes by tsunami data M_i of 9 or over. This may be arguing in a circle, as tsunami data were used to determine the magnitudes, however in the latter half of the twentieth century, all "severe" or giant tsunamis had moment magnitudes of 9 or greater. Also in the twentieth century, giant tsunamis had source areas or rupture areas with the main axes longer than 550 km. We deduce from the data that the threshold for giant tsunamis are a moment magnitude M_w of 9 or over and a rupture area with the main axis longer than 500 km.

We can go further and deduce that major tsunamis, those transoceanic tsunamis that cause destruction spottily in a distant coastline, have a threshold at $M_w = 8$ and a rupture length of 200 km to 500 km.

SOURCE PARAMETERS OF DESTRUCTIVE LOCAL TSUNAMIS

Since 1974 seismic moments M_o of large earthquakes have been routinely calculated and published [15, [16], [17], [18], [19], [20], [21], [22], [23], [24], [25], [26], [27], [28], [29], [30], [31], [32]. From the data sets tsunamigenic earthquakes [1] were selected; seismic moments M_o were converted to M_w; and the information was tabulated in Table 4. From this list, earthquakes with M_s or M_w greater than 8 were selected to compile information on rupture areas. As rupture areas of most of these earthquakes were already published by various investigators, we had to determine the rupture areas of only a few, namely the Tonga earthquake of 1977 and the McQuarie earthquake of 1989. As a check on previous results, we also determined rupture areas of a few more earthquakes.

Tonga Earthquake of June 22, 1977.

The Preliminary Determinations of Epicenters, Monthly Listings, published by the United States Geological Survey, were consulted to ferret out the aftershocks of this earthquake. In the month following the earthquake, only nine earthquakes were listed for the Tonga region. These nine were plotted (Figure 3), but only six were judged to be aftershocks. This gave an aftershock area of 160 km by 80 km.

Chile Earthquake of March 3, 1985 and the Andreanof Island Earthquake of May 7, 1986.

We publish our findings on these two earthquakes because of significant differences from

previously published results. In our study the rupture areas were determined by the inversion of body wave data, as refined by Yoshida [33], [34], [35]. As details of these analyses were published elsewhere [36], we shall give the results only. For the 1985 Chile earthquake, an uplift zone extends for 320 km with a width of roughly 80 km (Fig. 4, upper). Choy and Dewey [37] calculated a rupture area of 90 km by 10 km. For the Andreanof Island earthquake the uplift zone is 120 km by 80 km (Fig. 4, lower). As a check on the body wave analyses, Rayleigh waves R1 and R2 from the Andreanof Island earthquake were analyzed by the method proposed by Ben-Menahem [38]. The Rayleigh wave method gave a rupture length of less than 100 km [36]. On the other hand Boyd and Nabelek [39] found an aftershock area of 266 km by 110 km.

In the Andreanof Island earthquake of 1986 the discrepancy is between aftershock method on one hand and on the other hand seismic wave methods. For the Chile earthquake of 1985 the discrepancy occurs among seismic wave methods themselves. The discrepancies afford a topic for further study.

McQuarie Island Earthquake of May 23, 1989.

To determine the rupture area for this earthquake we used the aftershock method. The plot of earthquakes near McQuarie Island in the month following the earthquake is shown in Figure 5. What we judged to be aftershock area, enclosed by dashed lines, has dimensions of 250 km by 150 km.

Source Parameters of Earthquakes Generating Local Tsunamis.

Table 4 can be considered to be a rather inclusive list of tsunamigenic earthquakes in the Pacific Area since 1974. Notice that none of the earthquakes had a surface wave magnitude or moment magnitude greater than 8.5. None of the calculated rupture areas had a rupture length longer than 300 km, and none of the ensuing tsunamis caused damage at distant shores.

DISCUSSIONS

Classification of Tsunamis

From the numerical values of Tables 1, 2 and 3, we classify tsunamis according to M_w and size of source areas:

Giant tsunami:	$M_w \geq 9.1$.
	Rupture length > 550 km.
Major tsunami:	$8.4 < M_w < 9$.
	240 km $<$ Rupture length < 550 km.
Local tsunami:	$M_w < 8.4$.
	Rupture length < 240 km.

However, such neat divisions are not practicable as magnitude determinations have errors of $\pm$ 0.25 and rupture length determinations can be in error of 100 km. These criteria should be considered as guidelines to judge the size of tsunamis. Relaxing the above criteria, a more practical approach towards tsunami classification may be the following:

A. If M_w of the generating earthquake is greater than 8.7, and if the source length has

been found to be greater than 500 km, the chances of a giant tsunami are high.

B. If M_w is between 8 and 8.7, and the rupture length is under 500 km, the tsunami will probably be a major one.

C. If M_w is less than 8 and the rupture length is under 250 km, the tsunami is probably of local destructiveness.

Sometimes moment magnitude and source area information may not be consistent. None of the cases we have examined had such inconsistency, but it may occur. In that case the deciding factor will be source area length. For example if M_w was calculated to be 7.5 but the source area had a length of 500 km, the tsunami will probably be a giant one.

Time and Space Distribution of Tsunamigenic Earthquakes

In scanning the tables, odd patterns of geographical and temporal distributions of tsunamigenic earthquakes were noticed. Giant tsunamis were generated during the period from 1800 to 1990 from the following subduction zones: Kamchatka, Aleutian Islands, Gulf of Alaska, and Chile. Although the Japanese Islands subduction zone generated furious local tsunamis, such as the Sanriku earthquakes of 1896 and 1933 and the Nankaido earthquake of 1946, tsunami destruction has been limited to the Japanese Islands. Even in the Bonin Islands, roughly 1000 km from the Japanese Islands, the only Japanese tsunami that caused a significant runup height (4.5 m) was that generated by the Tokaido earthquake of 1854. In Hawaii damage from that tsunami was categorized as "none".

Other subduction zones where destructive transoceanic tsunamis, whether major or giant, have not been generated during the 190-year period from 1800 to 1990 are those in the southwest Pacific area, the west coast of North America from Canada to Mexico, and the Ecuador-Colombia section of the west coast of South America. But these regions have had very destructive local tsunamis.

The temporal distribution of large tsunamigenic earthquakes has an odd, but significant, pattern. Large earthquakes with moment magnitudes greater than 9 and generating giant tsunamis clustered in time during the 41-year period from 1837 to 1877 and during the 19-year period from 1946 to 1964. During the 68-year period from 1878 to 1945, there has been no giant tsunami. And since 1964 there has been no tsunamigenic earthquake with M_w greater than or equal to 9.

There is another odd pattern. During the nineteenth century and well into the twentieth century, although there were many destructive local tsunamis, there has been no major or giant tsunami originating in the Aleutian and Alaskan subduction zones, whereas in the twentieth century 3 of the 5 giant tsunamis have originated in these zones. As the Alaska-Aleutian Region contains recognizable subduction zones [40], the giant tsunami distribution may indicate a time dependent energy release pattern, which is a challenging problem to pursue [41], [42].

Are Aftershock Areas Equivalent to Rupture Areas?

Another matter that should be considered is the inconsistency in some cases between the aftershock area and the earthquake rupture area as determined by seismic waves and by retracing tsunami wavefronts. The salient case is the earthquake and tsunami of 1946 in the Aleutians, where the aftershock area was only 160 km by 120 km [11], while retracing tsunami wavefronts gave a tsunami source area of 570 km by 260 km. The other prominent case is the earthquake and tsunami of May 7, 1986 near Andreanof Islands, where the aftershock area was 260 km by 160 km [39], while seismic body wave and Rayleigh wave analyses gave a rupture length in the

range of 100 km. There is also a discrepancy between the aftershock area of the November 4, 1952 (1030 km x 240 km, [43]) and the rupture length as determined by Rayleigh waves (700 km, [44]). It has been taken for granted among seismologists that aftershock area outlines the fault rupture dimensions of an earthquake. Examination of data for tsunamigenic earthquakes have uncovered a few cases where the differences in the lengths of the long axis of the aftershock area and the rupture length are significant and not within the limits of error. The case of the earthquake and tsunami of 1946 may be explained on the grounds that the earthquake recording system in 1946 was inadequate for the purpose of aftershock area determination. Another source of difference may be the judgment of seismologists in deciding which earthquakes are aftershocks and which are earthquakes from a neighboring tectonic process. But as there were cases of discrepancy, the assumption of equating aftershock area with rupture area should be questioned and the problem thoroughly investigated.

CONCLUSIONS

The present study concludes that from the earthquake source parameters of moment magnitude and rupture area, we can distinguish among giant tsunamis, major tsunamis, and local tsunamis. The critical numbers are moment magnitude 9 and rupture length of 500 km, which are the thresholds for giant tsunamis. The other numbers are moment magnitude 8 and rupture length of 200 km, which define the threshold for major tsunamis. Lesser values are appropriate to locally destructive tsunamis or non-destructive tsunamis.

IMPLICATIONS FOR TSUNAMI WARNING AND ALERT

Rather obviously response plans to tsunamis should be tailored to the size of the tsunamis. Response plans based on worst case scenarios are appropriate for giant tsunamis, but such plans would be an overreaction for major tsunamis, wherein damage would be limited to selected places.

This study has shown that classes of tsunamis are correlatable to moment magnitude and tsunami source area. If these parameters can be determined within the time constraint of a tsunami alert, then decisions can be made on response plans. Can these parameters be determined within the allotted time?

At the present state of science and art, it takes a much longer time than available during a tsunami alert to determine M_o and hence M_w. In place of M_w, however, its equivalent called mantle magnitude as proposed by Talandier and Reymond [45] should be determined and used. Some seismic observatories may not be equipped even to determine mantle magnitude. In that case, as the Polynesian Geophysical Laboratory at Papeete, Tahiti, routinely determines mantle magnitude for large earthquakes, a quick long distance call to the laboratory will provide the needed information.

As for tsunami source area or the earthquake rupture area, the P wave inversion method (Fig. 4) can perform the task. As travel time of P waves even to stations at distance of 105 degrees (11,500 km) is about 15 minutes and as the P wave inversion method can be done in about 20 minutes, the earthquake rupture area is determinable within the time constraint, provided that personnel and facilities for such determinations have been set up.

The next question is: Who should be responsible for the source area determinations? The Pacific Tsunami Warning Center or the various regional emergency management agencies? Ideally the Center and the agencies should do the task so that there can be second opinion and cross checks. The main burden, however, rests with the regional emergency management agencies. The Center has responsibility to the Pacific-wide community and is an operational agency. Before a real-time source area determination system becomes operational, much research is necessary. The regional emergency management agencies can readily tap the resources of nearby seismological research organizations if the agencies can provide funds. Hence the regional emergency management agencies are the more appropriate locus for the source parameter determinations.

In this present day when real-time seismograph data are available from distant stations, carrying out the task is not insurmountable. Cooperating seismologists should be provided with telecommunications gear and computers so that the task can be done. The budget needed for the hardware is very affordable.

In any inversion method, a rough preliminary solution is assumed and entered as part of the input. The inversion method then refines the solution to obtain the best fit to the data. Prior research should be carried out to have a catalog of rough preliminary solutions for future earthquakes that may occur along the subduction zones with potential for tsunami generation. If preliminary solutions are available, inversion can proceed rapidly and be done within the time constraint.

Once the rupture area has been calculated from seismic data, the emergency management agency should call on its file of pre-calculated tsunami propagation charts and runup charts and plan for response measures at the critical places. Should the Pacific Warning Center issue a warning, then the emergency management agency is ready to swing into action.

The pre-calculated tsunami propagation charts and runup charts can be produced at rather affordable rates. Today seismological research has so progressed that the seismic gaps and potential tsunami producing seismic areas in the Aleutian Islands, Alaska, Kurile Islands, Japan, and Kamchatka regions can be identified [40]. From this information, expected tsunami wavefronts from seismic gaps and potential tsunami generators can be calculated. The calculated propagation charts can be stored on file to be tapped whenever a potential tsunamigenic earthquake has occurred in the North Pacific subduction zones.

ACKNOWLEDGMENTS

This project was initiated during a long term visit to the Meteorological Research Institute of Tsukuba City, Japan, under the auspices of National Science Foundation Grant INT 89-02219. Gratitude is expressed to Masami Okada and Masaaki Seino, the hosts at the Meteorological Research Institute for their kindness and assistance during the visit. The author thanks Yoshimitsu Okada of the Disaster Prevention Research Institute of Tsukuba City, Japan, for providing surface wave data and Shingo Yoshida of Tokyo Gakugei University for cooperation in determining source area parameters for two of the earthquakes mentioned in the paper.

The project was also assisted by funding from the Office of the Director of Civil Defense, State of Hawaii. George Curtis, presently at the University of Hawaii at Hilo, has kindly reviewed this manuscript and his comments were incorporated. This is School of Ocean and Earth Science and Technology Contribution no. 2686.

REFERENCES

[1] Utsu, T., 1990. Sekai Higai Zisin no Hyo. (Table of Destructive Earthquakes of the World.) Self publication, Tokyo, Japan, 243 pp.
[2] Iida, K., D. C. Cox and G. Pararas-Carayannis, 1967. Preliminary Catalog of Tsunamis Occurring in the Pacific Ocean. Haw. Inst. Geophys. Tech. Rept. No. 67-10, Univ. Hawaii.
[3] Soloviev, S. L., and Ch. N. Go, 1984 a. Catalogue of Tsunamis on the Eastern Shore of the Pacific Ocean. (translation from the Russian version.) Canada Inst. for Sci. and Techn. Info, Nat. Res. Council, Ottawa, Ontario, Canada. 285 pp.
[4] Soloviev, S. L. and Ch. N. Go, 1984 b. Catalogue of Tsunamis on the Western Shore of the Pacific Ocean. (translation from the Russian version.) Dept. of Fisheries and Oceans, Sidney, B. C., Canada. 439 pp.
[5] Lander, J. F., and P. A. Lockridge, 1989. United States Tsunamis (including United States Possessions). Nat. Geophys. Data Center, Boulder, Colo. 265 pp.[9] Abe, K., 1979. Physical size of great earthquakes of 1837-1974 inferred from tsunami data. J. Geophys. Res. vol. 84, 1561-1568.
[6] Pararas-Carayannis, G., 1969. Catalog of Tsunamis in the Hawaiian Islands. World Data Center A, Tsunamis, Envr. Sci. Surv. Agency, 94 pp.
[7] Shepard, F. P., G. A. Macdonald and D. C. Cox, 1950. The tsunami of April 1, 1946. Bull. Scripps Inst. Oceanography Vol. 5, 391-527.
[8] Hatori, T., 1989. Characteristics of tsunamis associated with aftershock and swarm near Japan. Zisin, ser. 2, vol. 42, 183-188.
[9] Abe, K., 1979. Physical size of great earthquakes of 1837-1974 inferred from tsunami data. J. Geophys. Res. vol. 84, 1561-1568.
[10] Bolt, B., 1988. Earthquakes. W. H. Freeman and Co., San Francisco. 282 pp.
[11] Sykes, L. R., 1971. Aftershock zones of great earthquakes, seismicity gaps, and earthquake prediction for Alaska and the Aleutians. J. Geophys. Res., vol. 76, 8021-8041.
[12] Hatori, T., 1981. Tsunami magnitude and source area of Aleutian-Alaska tsunamis. Earthq. Res. Inst. Bull., vol. 56, 97-110.
[13] Bodle, R. R., 1946. Note on the earthquake and seismic sea wave of April 1, 1946. Am. Geophys. Un. Trans., vol. 27, 464-465.
[14] Green, C. C., 1946. Seismic sea wave of April 1, 1946, as recorded on tide gauges. Am. Geophys. Un. Trans., vol. 27, 490-500.
[15] Dziewonski, A. M., A. Friedman, D. Giardini and J. H. Woodhouse, 1983. Global seismicity for 1982: centroid moment tensor solutions for 308 earthquakes. Phys. Earth Planet. Int., vol. 33, 76-90.
[16] Dziewonski, A. M., J. E. Franzen and J. H. Woodhouse, 1985. Centroid-moment tensor solutions for July-September, 1984. Phys. Earth Planet. Int., vol. 38, 203-213.
[17] Dziewonski, A. M., J. E. Franzen and J. H. Woodhouse, 1986. Centroid-moment tensor solutions for July-September, 1985. Phys. Earth Planet. Int., vol. 42, 205-214.
[18] Dziewonski, A. M., G. Ekstrom, J. E. Franzen, 1987. Global seismicity of 1977; centroid-moment tensor solutions for 471 earthquakes. Phys. Earth Planet. Int., vol. 45, 11-36.
[19] Dziewonski, A. M., G. Ekstrom, J. E. Franzen, and J. H. Woodhouse, 1987. Centroid-moment tensor solutions for January-Mach 1986. Phys. Earth Planet. Int., vol. 45, 1 - 10.
[20] Dziewonski, A. M., G. Ekstrom, J. E. Franzen, and J. H. Woodhouse, 1987. Centroid-moment tensor solutions for April-June 1986. Phys. Earth Planet. Int., vol. 45, 229-239.
[21] Dziewonski, A. M., G. Ekstrom, A. Friedman, and J. H. Woodhouse, 1987. Global seismicity of 1978: centroid moment tensor solutions for 512 earthquakes. Phys. Earth Planet. Int., vol. 46, 316-342.
[22] Dziewonski, A. M., G. Ekstrom, J. H. Woodhouse, and G. Zwart, 1989. Centroid-moment tensor solutions for July-September, 1988. Phys. Earth Planet. Int., vol. 56, 165-180.
[23] Dziewonski, A. M., G. Ekstrom, J. H. Woodhouse, and G. Zwart, 1989. Centroid-moment tensor solutions for October-December, 1987. Phys. Earth Planet. Int., vol. 54, 10-21.
[24] Dziewonski, A. M., G. Ekstrom, J. H. Woodhouse and G. Zwart, 1990. Centroid-moment tensor solutions for April-June 1989. Phys. Earth Planet. Int., vol. 60, 243-253.
[25] Person, W. J., 1987. Seismological notes. Bull. Seis. Soc. Am., vol. 77, 682-687.
[26] Person, W. J., 1987. Seismological notes. Seis. Soc. Am. Bull., vol. 77, 1486-1496.

[27] Person, W. J., 1988. Seismological notes. Seis. Soc. Am. Bull., vol. 78, 390-398.
[28] Person, W. J., 1988. Seismological notes. Seis. Soc. Am. Bull., vol. 78, 1390-1395.
[29] Person, W. J., 1988. Seismological notes. Seis. Soc. Am. Bull., vol. 78, 1624-1626.
[30] Person, W. J., 1988. Seismological notes. Seis. Soc. Am. Bull., vol. 78, 1837-1846.
[31] Person, W. J., 1989. Seismological notes. Seis. Soc. Am. Bull., vol. 79, 225-228.
[32] Person, W. J., 1990. Seismological Notes. May-June 1990. Seis. Soc. Am. Bull., vol. 80, 498-502.
[33] Yoshida, S., 1986 A method of waveform inversion for earthquake rupture process. J. Phys. Earth, vol. 34, 235-255.
[34] Yoshida, S.,1989. Waveform inversion using ABIC for the rupture process of the 1983 Hindu Kush earthquake. Phys. Earth Planet. Int., vol. 56, 389-405.
[35] Yoshida, S., 1991. Waveform inversion for rupture process using a non-flat seafloor model: application to 1986 Andreanof Islands and 1985 Chile earthquakes. Tectonophysics (submitted).
[36] Furumoto, A. S., and S. Yoshida, 1990. Fast determination of tsunami generation mechanism. Pacon 90, Proc. 4th Pac. Cong. Mar. Sci. Tech., vol. 1, 151-155.
[37] Choy, G. L., and J. W. Dewey. 1988. Rupture process of an extended earthquake sequence: Teleseismic analysis of the Chilean earthquake of March 3, 1985. J. Geophys. Res., vol. 3, B2, 1103-1118.
[38] Ben-Menahem, A., 1961. Radiation of seismic surface waves from finite moving sources. Bull. Seism. Soc. Am., vol. 51, 401-435.
[39] Boyd, T. M., and J. L. Nabelek, 1988. Rupture process of the andreanof islands earthquake of May 7, 1986. bull. Seism. Soc. Am., vol. 78, 1653-1673.
[40] McCann, W. K., S. P. Nishenko, L. R. Sykes and J. Krause, 1979. Seismic gaps and plate tectonics: seismic potential for major boundaries. Pure Appl. Geophys., vol. 117, 1 - 56.
[41] Abe, K., 1973. Tsunami and mechanism of great earthquakes. Phys. Earth Planet. Int., vol. 7, 143-153.
[42] Kanamori, H., 1977. The energy release in great earthquakes. J. Geophys. Res., vol. 82, 2981 -2987.
[43] Bath, M., and H. Benioff, 1958. Aftershock sequence of the Kamchatka earthquake of November 4, 1952. Bull. Seism. Soc. Am., vol. 48, 1-15.
[44] Ben-Menahem, A., and M. N. Toksoz, 1963. Source mechanism from spectrums of long-period surface waves. 2. The Kamchatka earthquake of November 4, 1952. J. Geophys. Res., vol. 68, 5207-5222.
[45] Talandier, J., and D. Reymond, 1988. A new approach for a quick estimation of seismic moment magnitude, Mm. Natural and Man Made Hazards, an International Conference, Reidel and Co. 109-124.
[46] Hatori, T., 1967. The generating area of Sanriku Tsunami of 1896 and its comparison with the tsunami of 1933. Zisin, ser. 2, vol. 20, 164-170.
[47] Christensen, D. H., and L. J. Ruff, 1986. Rupture process of the March 3, 1985, Chilean earthquake. Geophys. Res. Lett. vol. 13, no. 8, 721-724.
[48] Lay, T., L. Astiz, H. Kanamori and D. H. Christensen, 1989. Temporal variation of large intraplate earthquakes in coupled subduction zones. Phys. Earth Planet. Int., vol. 54, 258-312.
[49] Hutchinson, R. O., 1954. The Kamchatka earthquake of November 1952. Earthquake Notes, vol. 25, 37-41.
[50] Carr, M., 1977. Volcanic activity and great earthquakes at convergent plate margins. Science, vol. 197, 655-657.
[51] Wada, T., T. Furuzawa and H. Ono, 1963. Source-mechanism of the Chilean earthquake from spectra of long-period surface waves. Zisin, Ser. 2, vol. 16, 181-187.
[52] Press, F., A. Ben-Menahem and M. N. Toksoz, 1961. Experimental determination of earthquake fault length and rupture velocity. J. Geophys. Res., vol. 66, 3471-3485.
[53] Pflaker, G., 1964. Tectonics of March 27, 1964, Alaska Earthquake. U. S. Geol. Surv. Prof. Paper, 543-1.
[54] Furumoto, A. S., 1967. Source mechanism of the Alaska earthquake and tsunami of March 27, 1964. Part II. Rayleigh waves. Pac. Sci., vol 21, 311-316.
[55] Pararas-Carayannis, George, 1967. A study of the source mechanism of the Alaska earthquake and tsunami of March 27, 1964: Part 1, Water waves. Pac. Sci., vol. 21, 301-310.
[56] Hatori, T., 1976. Wave source of the Hawaii tsunami in 1975 and the tsunami behavior in Japan. Zisin, Ser. 2, vol. 29, 355-364.
[57] Furumoto, A. S., and R. Kovach, 1979. The Kalapana earthquake of November 29, 1975: an intraplate earthquake and its relation to geothermal processes. Phys. Earth Planet. Int., vol. 18, 197-208.
[58] Beck, S. L., and L. J. Ruff, 1984. The rupture process of the Great 1979 Columbia earthquake: Evidence for the asperity model. J. Geophys. Res., vol. 69, B 12, 9281-9291.

[59] Stewart, G. S., and S. N. Cohn, 1979. The 1976 August 16, Mindanao, Philippines earthquake (Ms = 7.8) - evidence for a subduction zone south of Mindanao. Geophys. J. Roy. Astron. Soc., vol. 57, 51-65.
[60] Fitch, T. J., R. G. North and M. W. Shields, 1981. Focal depths and moment tensor representations of shallow earthquakes associated with the Great Sumba Earthquake. J. Geophys. Res., vol. 86, B10, 9357-9374.
[61] Mendoza, C., and J. W. Dewey, 1984. Seismicity associated with the Great Colombia-Ecuador Earthquake of 1942, 1958, and 1979. Implications for barrier models of earthquake rupture. Bull. Seism. Soc. Am., vol. 74, 577-594.
[62] Satake, K., 1985. The mechanism of the 1983 Japan Sea earthquake as inferred from long-period surface waves and tsunamis. Phys. Earth Planet. Int., vol 37, no. 4, 249-260.
[63] Satake, K., 1989. Inversion of tsunami waveforms for the estimation of heterogeneous fault motion of large submarine earthquakes: The 1968 Tokachi-oki and 1983 Japan Sea earthquakes. Jour. Geophys. Res. vol. 94, no. B5, 5627-5636.
[64] Lomnitz, C., 1988. The 1985 Mexico earthquake. in Natural and Man-Made Hazards, an International conference, Rimouski, Canada, Reidel Pub. Co., 63-79.
[65] Beck, S. L., and L. J. Ruff, 1985. The rupture process of the 1976 Mindanao earthquake. J. Geophys. Res. vol. 90, 6773-6782.

TABLE 1.
DESTRUCTIVE TRANSOCEANIC TSUNAMIS

Year	Mo-Day	Source Location	Affected Areas	Tsunami Heights (meters)	Damage in Hawaii (1)	Tsunami Mag. m	Size
1837	Nov 7	Valdivia, Chile	Hawaii Mangareva Samoa Japan	2.5 to 6 3 0.6 1 to 2	Severe	3	Giant
1841	May 17	Kamchatka	Hawaii Japan	1 to 4 1 to 2	Small	2	Major
1854	Dec 23	Tokaido, Japan	Bonin Islands	4.5	None	4	Major
1868	Aug 13	Arica, Chile	Hawaii Japan New Zealand	2 to 4.5 2 to 3 3 to 4	Severe	4	Giant
1869	Jul 24	So. Pacific ?	Hawaii	4.6 to 5.5	Moderate		Major
1877	May 10	Iquique, Chile	Hawaii Japan New Zealand	3 to 4.8 2 to 3 1 to 2	Severe	4	Giant
1896	June 15	Sanriku, Japan	Hawaii Bonin US West Coast	3 to 5.5 1 1.5	None	4	Major
1906	Aug 17	Central Chile	Hawaii San Pedro, Cal.	1.5 to 3.6 1.8	Small	2	Major
1923	Feb 3	Kamchatka	Hawaii Japan	3.7 to 6.1 0.5 to 1.8	Small	3	Major
1933	Mar 2	Sanriku, Japan	Hawaii	3 to 3.3	Small	3	Major
1946	Apr 1	East Aleutians	Hawaii US West Coast Japan Marquesas	10 to 16 2 to 3 0.5 to 1 9 to 10	Severe	5	Giant
1952	Nov 4	Kamchatka	Hawaii Japan Aleutians US West Coast	0.8 to 9.1 2 to 3 1.5 1 to 1.4	Severe	4	Giant
1957	Mar 4	Adak, Aleutians	Hawaii US West Coast Japan	10 to 16 1.5 0.5 to 1	Severe	3.5	Giant

1960	Mar 22	Chile	Hawaii	5 to 10	Severe	4.5	Giant
			Japan	3 to 4			
			US West Coast	1 to 1.7			
			Samoa	1 to 2.4			
1964	Mar 28	Alaska	Hawaii	3.5 to 4.6	Severe	4.5	Giant
			US West Coast	3.5 to 4.5			
			Japan	1 to 1.5			

(1) Classification for tsunamis up to 1946 found in [7], after 1946 was done by present author. Data were assembled from [2], [3], [4], [5], [6], [7], [8] and [9].

TABLE 2.
SOURCE PARAMETERS OF DESTRUCTIVE TRANSOCEANIC TSUNAMIS

Year	Mo-Day	Location	Depth (km)	Tsunami Size	Ms	Mw	MI [9]	Source Area (km x km)	Ref.
1837	Nov 7	Chile		Giant	8.5		9.3		
1841	May 17	Kam-chatka	30	Major	8.4		9		
1854	Dec 23	Japan		Major	8.4		8.3		
1868	Aug 13	Chile		Giant	8.5		9		
1869	Jul 2	S. Pac ?		Major					
1877	May 10	Chile		Giant	8.5		9		
1896	Jun 15	Japan	Shallow	Major	7.6		8.6	430 x 120, (T)	[46]
1906	Aug 17	Chile	Shallow	Major	8.4	8.2	8.4	360 x 120, (A)	[46]
1923	Feb 3	Kam-chatka	40	Major	8.3	8.3	8.8	240 x 120, (T)	[48]
1933	Mar 2	Japan	0 - 20	Major	8.4	8.4	8.3	530 x 165, (T)	[46]
1946	Apr 1	Aleutians	Shallow	Giant	7.4		9.3	180 x 100, (A)	[11]
								400 x 140, (T)	[12]
								570 x 260, (T)	*
1952	Nov 4	Kam-chatka	30 - 60	Giant	8.3	9	9	1030 x 240, (A)	[43]
								675 x 240, (A)	[49]
								700 x ?, (S)	[44]
1957	Mar 9	Aleutian	Normal	Giant	8.1	9.1	9	1220 x 145, (A)	[39]
1960	Mar 22	Chile	Normal	Giant	8.5	9.5	9.4	950 x 240, (A)	[50]
								1200 x ?, (S)	[51]
								1300 x ?, (S)	[52]
1964	Mar 28	Alaska	33	Giant	8.4	9.2	9.1	500 x 100, (A)	[53]
								800 x 150, (S)	[54]
								800 x 150, (T)	[55]

Data in Depth column were compiled from [2]. Keys to Source Area column. A = aftershock data; S = inversion of seismic wave data; T = retracing tsunami data. In Reference column, * = this paper.

TABLE 3.

ARRIVAL TIMES AND TRAVEL TIMES OF THE TSUNAMI OF APRIL 1, 1946
Origin time of earthquake was 1946 April 1, 12h 29m, G. C. T.

TIDE STATION	ARRIVAL TIME	TRAVEL TIME
Sitka	April 1, 15 h 05 m	2 h 36 m
Yakutat	April 1, 15 h 08 m	2 h 39 m
Crescent City	April 1, 17 h 16 m	4 h 47 m
La Jolla	April 1, 18 h 44 m	6 h 15 m
Valparaiso	April 2, 06 h 38 m	18 h 09 m

TABLE 4.
SOURCE PARAMETERS OF EARTHQUAKES
GENERATING LOCAL TSUNAMIS

Year	Date	Location	Depth (km)	Ms	Mw	Rupture Dimensions (km x km)	References
1974	Sep 27	Kuriles	45	7.6			
1975	Jul 20	Papua N-G	49	7.6	7.9		
1975	Oct 31	Philippines	50	7.6			
1975	Nov 29	Hawaii	7	7.2	7.5 [58]	60 x 40	[56]
1976	Jan 14	Kermadec	33	7.9	8.2	240 x 180	[48]
1976	Aug 14	Mindanao		8.0	8.15	160 x 80	[65, 59]
1977	Apr 2	Samoa	33	7.6	7.3		
1977	Apr 21	Solomons	33	7.2	7.4		
1977	Jun 22	Tonga	65	7.2	8.1	190 x 105	*
1977	Aug 19	Sumbawa	3	8.0	8.4	160 x 80	[60]
1978	Jun 12	Japan	40	7.5	7.7		
1978	Nov 29	Mexico	49	7.8	7.8		
1979	Sep 12	West Irian	33	7.9	7.6		
1979	Nov 16	Fiji	33	6.9	6.8		
1979	Dec 12	Colombia	32	7.9	8.1	235 x 135	[58, 61]
1980	Jul 17	Solomon	30	7.9	7.8		
1981	Sep 1	Samoa	20	7.7	7.5		
1982	Mar 21	Japan	40	7.1	6.9		
1982	Dec 19	Tonga		7.7	7.5		

1983	Mar 18	Papua N-G	88	7.8	7.7		
1983	May 26	Japan	14	7.8	7.9	130 x 45	[62, 63]
1983	Oct 4	Chile	31	7.3	7.4		
1984	Aug 7	Japan	33	7.1	6.9		
1985	Mar 3	Chile	<33	7.8	7.9	280 x 140 90 x 10	* [37]
1985	Jul 3	Papua N-G	37	7.2	7.2		
1985	Sep 19	Michoacan	16	8.1	8.0	90 x 90	[64]
1986	May 7	Andreanof	19	7.7	8.0	120 x 100	*
1986	May 17	Andreanof	<33	6.6	6.5		
1986	Oct 20	Kermadec	29	8.2	7.5	170 x 80	[48]
1987	Mar 5	Chile	<33	7.3	7.6		
1987	Jul 6	Vanuatu	<33	6.6	6.6		
1987	Oct 5	Tonga	16	7.3	7.3		
1987	Oct 12	Solomons	<33	6.9	7.0		
1987	Oct 16	Papua N-G	<33	7.5	7.1		
1987	Nov 17	Alaska	8	7.0	7.2		
1987	Nov 26	Indonesia	<33	6.5	6.5		
1987	Nov 30	Alaska	10	7.6	7.8		
1988	Mar 6	Alaska	10	7.6	7.3		
1988	Jul 5	Papua N-G	63	6.8	6.8		
1988	Aug 10	Solomon	38	7.4	7.2		
1989	May 23	Macquarie	109	8.2	8.2	250 x 150	*
1989	Jun 26	Hawaii	9	6.1	6.5		
1989	Oct 18	Loma Prieta, U.S.	19	7.1	6.9		

* Results of this paper.

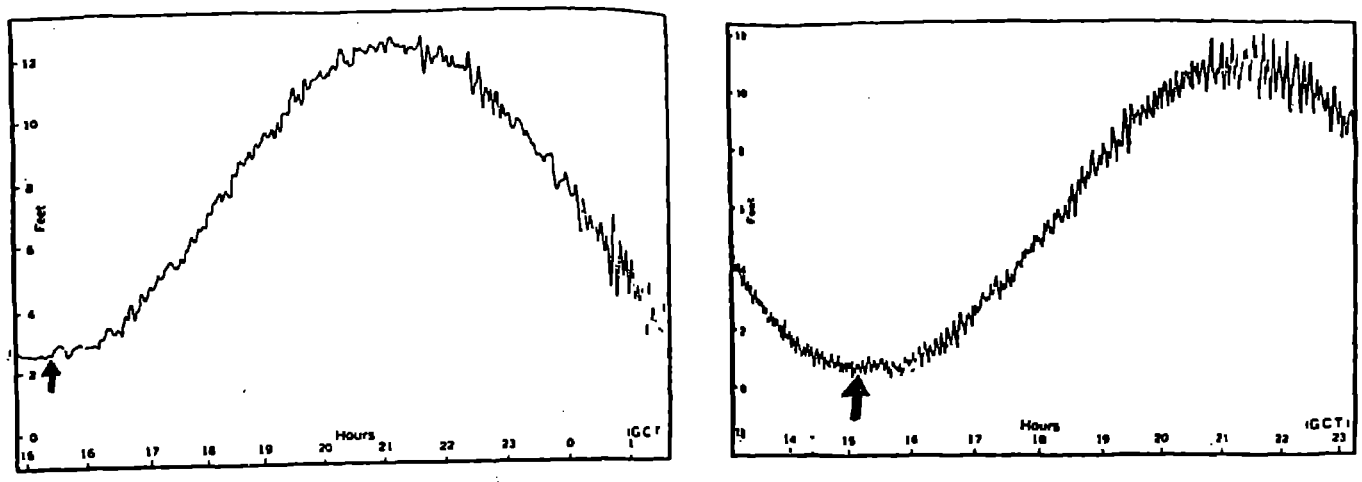

Figure 1. Tide gage records from Sitka (left) and Yakutat (right). Arrows indicate the arrival times of the Aleutian tsunami of April 1, 1946. Records were originally published by Bodle (1946) without indication of arrival times.

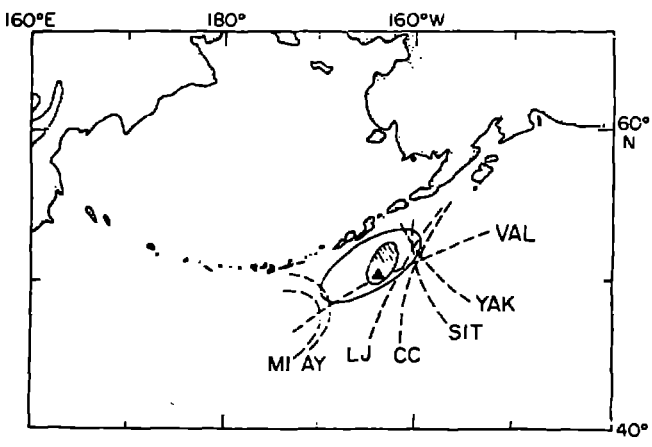

Figure 2. Retracing waves to origin for the Aleutian tsunami of April 1, 1946. MI is the wave retraced from Miyako, Japan (Hatori, 1981); AY from Ayukawa, Japan (Hatori, 1981); LJ from La Jolla; CC from Crescent City; SIT from Sitka; YAK from Yakutat; and VAL from Valparaiso. The solid line ellipse outlines the tsunami source; the hatchured ellipse, the aftershock area. The triangle is the epicenter of the generating earthquake.

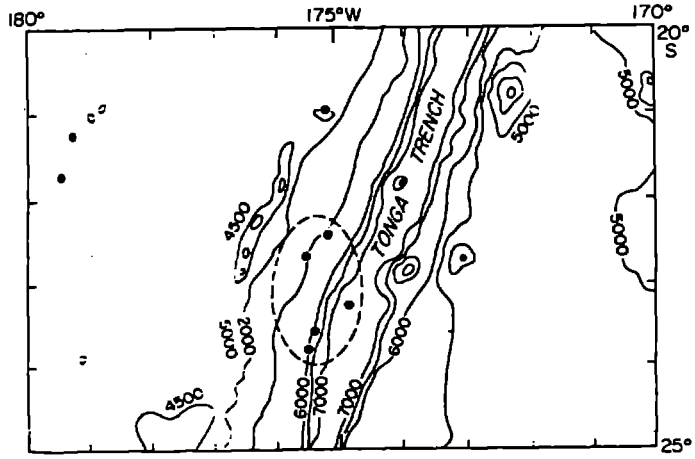

Figure 3. Aftershock area of the Tonga earthquake of June 22, 1977. Solid circles are earthquakes; the dashed line encloses the aftershock area.

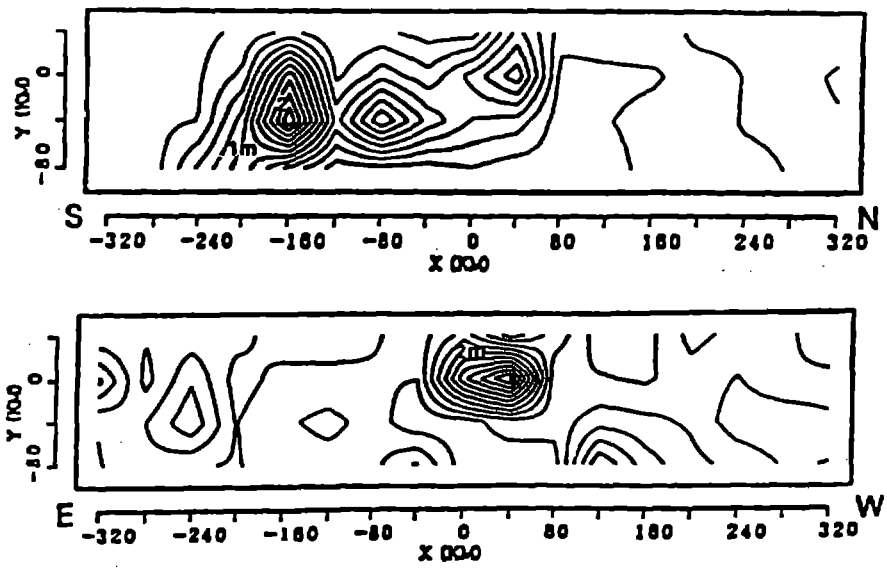

Figure 4. Slip contours of the Chile earthquake of 1985 (upper) and the Andreanof earthquake of 1986 (lower). Contours in the upper diagram are in intervals of 0.2 m; in the lower diagram the contours are in intervals of 0.5 m. From Furumoto and Yoshida, 1990.

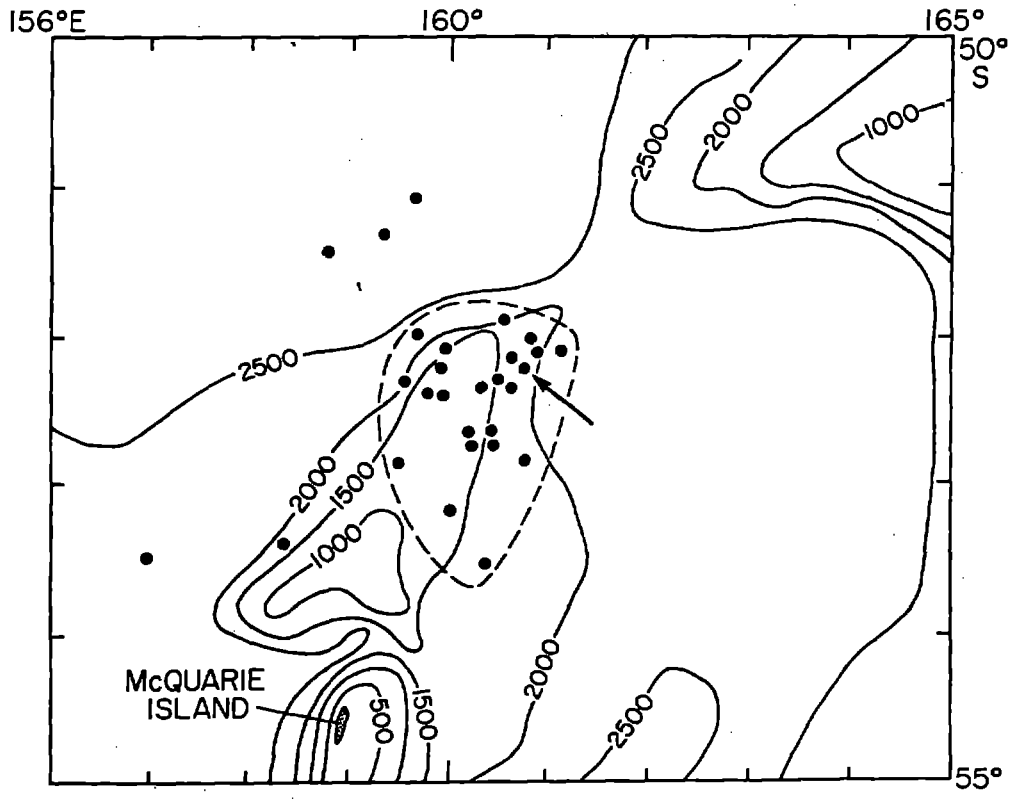

Figure 5. Aftershock area of the McQuarie earthquake of 1989. Solid circles are earthquakes; the dashed line encloses the aftershock area. Bathymetry are in meters.

10" or 25 cm

THE TSUNAMI SOCIETY

SCIENCE OF TSUNAMI HAZARDS

Publication Format for Camera-Ready Copy and Information for Authors:

1. Typing area shown by border.

2. One-column text.

3 All text must be typed single-space. Indent 5 spaces to start a new paragraph.

4. Page numbers in lower right hand corner in pencil or blue marker.

5. Top half of first page to contain the title in capitals, followed by the authors and author affiliation, centered on page.

6. Bottom half of first page to contain the abstract with the heading ABSTRACT centered on page.

7. Author must also enclose a separate sheet containing:
   - name and mailing address of senior author
   - one or two suggested index subjects
   - three to five keywords for cataloging
   - statement of any other submittal, publication, or presentation

8. Send original and a copy, with above information, to:

Dr. Tad Murty, Editor
Institute of Ocean Sciences
Box 6000
Sidney, B.C., V8L 4B2
CANADA

7½" or 19 cm

ANALYTICAL THEORY FOR TSUNAMI RUN UP ON A SMOOTH SLOPE

V. M. Kaistrenko, R. Kh. Mazova,
E. N. Pelinovsky, and K. V. Simonov

Institute of Applied Physics, Academy of Sciences of the USSR
Gorky, USSR

The description of the tsunami run-up is of greatest importance for tsunami zonation and evaluation of tsunami hazard for hydrotechnical and coastal constructions. The difficulties arising here are evident: the complexity of coastal zone morphology and the variety of underlying surfaces changing due to their interaction with the water flows caused by tsunamis, the possibility of wave breaking, stream turbulization, and competition of nonlinear and dispersion effects. In this context the analytical theories for tsunami run-up acquire greater importance since they provide a means to show the effect of different factors, to obtain the run-up determining parameters, and to test the numerical algorithms for solving the equations involved. In this paper the analysis of non-breaking long waves run-up on an impermeable smooth slope is given. This situation is typical for tsunami waves initiated by underwater earthquakes with their lengths far exceeding the depth of a basin and the probability of breaking no higher than 0.5 [1,2] (at least up to the run-up height of 10 m). The obtained solutions were applied to improve the existing tsunami zonation map of the USSR Pacific coast.

As initial equations when no wave breaking takes place and dissipation is neglected, we take the nonlinear shallow water equations:

$$\begin{aligned} &\frac{\partial \eta}{\partial t}+u\frac{\partial u}{\partial x}+g\frac{\partial \eta}{\partial x}=0. \\ &\frac{\partial \eta}{\partial t}+\frac{\partial}{\partial x}[(h+\eta)u]=0 \end{aligned} \qquad (1)$$

Here η is water elevation U is depth averaged wave stream velocity, g is acceleration due to gravity, and $h(x)$ is the variable depth of the basin. It is assumed that $h(x) = -\alpha x$ with X axis directed to the shoreline and α = const. First we obtain the similarity criteria for set (1) from [3,4]:

$$t=\omega t,\ x=\frac{\alpha x}{H},\ \eta=\frac{\eta}{H},\ U=\frac{U\alpha}{\omega H}. \qquad (2)$$

where H and ω are typical wave height and wave frequency, respectively. In those variables set (1) has the following form (further the tildes are omitted):

$$\frac{\partial u}{\partial t}+U\frac{\partial u}{\partial x}+\frac{1}{Br}\frac{\partial \eta}{\partial x}=0$$
$$\frac{\partial \eta}{\partial t}+\frac{\partial}{\partial x}[(-x+\eta)u]=0 \qquad (3)$$

which contains only one dimensionless parameter,

$$Br = H\omega^2/g\alpha^2 \qquad (4)$$

Of course, the existence of only one similarity parameter is due to the neglect of some factors (dissipation, dispersion and others). This neglect under certain conditions can be employed when analyzing tsunamis. From that fact the similarity criterion for tsunami modelling in a hydraulic chute can be derived, the vertical and horizontal scale can be changed independently as long as the correlation between them fits conditions (4) (identical scale changing is not achieved due to large lengths of tsunami waves). It should be also stressed that the parameter *Br* is not related to the nonlinearity of system (3). It shows certain relationship between the solutions of linear and nonlinear problems which will be discussed further. Note also that the parameter *Br* appeared when particular solutions of set (3) [3] or experimental data [6,7] were analyzed. In this paper it is obtained from dimensional analysis. This fact confirms the fundamental importance of the parameter. Further it will be shown that this parameter determines the character of the tsunami run-up: quiet flooding on the shore or run-up of a broken wave.

In solving set (3) the transformation first introduced by Carrier and Greenspan [8] proves to be effective:

$$U = \frac{1}{Br}\frac{2}{\sigma}\frac{\partial \phi}{\partial \sigma},$$
$$\eta = \frac{1}{Br}\left[\frac{\partial \phi}{\partial \lambda} - \frac{2}{\lambda^2}\left(\frac{\partial \phi}{\partial \sigma}\right)^2\right], \qquad (5)$$
$$x = \frac{1}{Br}\left[\frac{\partial \phi}{\partial \lambda} - \frac{\sigma^2}{4} - \frac{2}{\sigma^2}\left(\frac{\partial \phi}{\partial \sigma}\right)^2\right].$$
$$t = \lambda - \frac{2}{\sigma}\frac{\partial \phi}{\partial \sigma}.$$

and set (3) becomes the linear wave equation

$$\frac{\partial^2 \phi}{\partial \lambda^2} - \frac{\partial^2 \phi}{\partial \sigma^2} - \frac{1}{\sigma}\frac{\partial \phi}{\partial \sigma} = 0. \qquad (6)$$

Note that the new variation σ is proportional to the absolute basin depth,

$$\sigma^2 = 4Br(\eta - x), \tag{7}$$

so that Eq. (6) is solved on the fixed semiaxis $0 \le \sigma \le \infty$ (with $\sigma = 0$ corresponding to a moving run-up boundary) unlike the varying region for (3).

Along with the nonlinear shallow-water equations consider the linear set

$$\begin{aligned} &\frac{\partial u}{\partial t} + \frac{1}{Br}\frac{\partial n}{\partial x} = 0. \\ &\frac{\partial \eta}{\partial t} + \frac{\partial}{\partial x}(-xu) = 0. \end{aligned} \tag{8}$$

If in the analysis of set (8) the linear variant of Carrier-Greenspan transformations [9] is used then

$$\begin{aligned} U &= \frac{2}{\sigma^2 Br}\frac{\partial \phi_0}{\partial \sigma_0}, \\ \eta &= \frac{1}{Br}\frac{\partial \theta_0}{\partial \lambda_0}, \\ x &= -\sigma_0^2/4Br, \quad t = \lambda_0 . \end{aligned} \tag{9}$$

Set (8) also reduces to the linear wave equation:

$$\frac{\partial^2 \phi}{\partial \lambda_0^2} - \frac{\partial^2 \phi_0^2}{\partial \sigma_0^2} - \frac{1}{\sigma_0}\frac{\partial \phi_0}{\partial \sigma_0} = 0, \tag{10}$$

where $\sigma_0 = 0$ corresponds to the shoreline. The comparison of linear and nonlinear problems appears to be useful for the tsunami run-up calculation as it will be shown below.

Consider the particular solution of Eq. (6) in the form,

$$\phi(\sigma,\lambda) = AJ_0(\sigma)\cos\lambda \tag{11}$$

where Jo is the Bessel function with zero index, A is an arbitrary constant and in analogy the solution of Eq. (10):

$$\phi_0(\sigma_0,\lambda_0) = A_0 J_0(\sigma_0)\cos\lambda_0 . \tag{12}$$

Assuming that a tsunami wave runs from a remote source ($\sigma \to \infty$) where it is linear we can say that the asymptotic forms (11) and (12) coincide and represent the superposition of two waves propagating in opposite directions:

$$\eta(x,t) = \frac{A}{2Br\sqrt{\pi}\sqrt[4]{|x|Br}}\left[\sin\left(\lambda + 2\sqrt{Br|x|} - \frac{\pi}{4}\right) + \sin\left(\lambda - 2\sqrt{Br|x|} - \frac{\lambda}{4}\right)\right] \tag{13}$$

Here the argument of the function $\lambda \pm 2\sqrt{Br|x|}$ is the "classical" argument

$t \pm \int [gh(x)]^{-1/2} dx$ and the wave amplitude changing according to Green's law as $|x|^{-1/4} \sim h^{-1/4}$ is equal to

$$H_0(x) = A/(2Br\sqrt{\eta}\sqrt[4]{|x|Br}). \tag{14}$$

It allows the determination of constant A through the initial wave height at the distance $|x|$ from the shoreline.

Solutions (11) and (12) are obtained through tsunami parameters in the open ocean and they permit estimation of wave field in all cases including wave climbing on the shore. In contrast to the solution of linear problem (12) the solution to the nonlinear one is not explicit and wave shape analysis is difficult. Consider the tsunami run-up characteristics which are of primary practical importance. Using function (11) for transformation (5) with $\sigma = 0$ we find the water boundary moving in the parametric form:

$$\begin{aligned} x &= \frac{-A}{Br}(\sin\lambda + \frac{A}{2}\cos^2\lambda), \\ t &= \lambda + A\cos\lambda. \end{aligned} \tag{15}$$

It is easy to determine from this expression the maximum range of the horizontal run-up $L_{max} = x_{max}$ or the height of the vertical run-up measured from the sea level:

$$R = A/Br \tag{16}$$

Substituting A from Eq. (14) we find relative strengthening:

$$\frac{R}{H_0(x)} = 2\sqrt{\pi}\sqrt[4]{|x|Br}. \tag{17}$$

Taking into account the importance of this formula we transform it using dimensional variables,

$$R/H_o = 2\pi\sqrt{\frac{2L_w}{\lambda}} \tag{18}$$

where L_w is the distance from the shoreline to the isobath h at which the initial wave amplitude was found, and $\lambda = 2\pi\sqrt{gh}/\omega$ is the wave length at the same place. It should be stressed that Eq. (18) is accurate within the nonlinear theory. Therefore the relative tsunami run-up height does not depend on the initial height and is determined by the correlation between the slope width and the wave length. Within the linear theory Eqs. (9) and (12) give the water level oscillations on the shoreline

$$\eta(0,t) = R \sin t. \tag{19}$$

where R is determined by Eqs. (16)-(18). Thus the maximum wave height on the shoreline in the linear theory coincides with the maximum vertical run-up height within the nonlinear theory. Thereby a "linear" method for estimating the run-up maximum

by the wave height on the shoreline can be suggested. This method has been used heuristically by many scientists [10,11,12]. The given comparison was introduced in [9] and actually verifies this approach.

The obtained results are true only with the uniqueness of the Carrier-Greenspan transformation, i.e., if the Jacobian $\partial(x,t)/\partial(\sigma,\lambda)$ does not converge to zero. If this condition is valid, the solution is everywhere smooth and this fact corresponds to tsunami non-breaking when the run-up is but a flooding on a beach. The mathematical condition of uniqueness has the form [8] $A = 1$ or with regard to (16) $R\,Br < 1$. We have not yet defined the characteristic height H to which the initial parameters are normalized. It is natural to choose for this characteristic height either the initial amplitude H_0 or the run-up height R and it is most convenient to choose R for the height scale taking into account dependence of H_0 on the distance to the shoreline. Then the dimensionless run-up height R is equal to unity and the condition $A < 1$ comes to the expression,

$$Br = \frac{R\omega^2}{g\alpha^2} < 1 \qquad (20)$$

(see Refs. [3,4,5,6,7]). Therefore the fundamental role of the run-up height determining the character of the process is clear. When the opposite condition $(Br < 1)$ is met within the nonlinear shallow-water theory, "the gradient catastrophe" must occur and the front slope of the wave must break. In practice the actual behavior of the wave with $Br > 1$ depends on the correlation between nonlinearity, dispersion and dissipation and is not necessarily followed by breaking. Nevertheless for brevity sake we call the condition $Br = 1$ the condition of breaking.

For every sloping beach characterized by the tangent α of the slope angle, the critical run-up height is obtained. If the run-up height is more than critical, then breaking must take place. This value depends on the wave period $T = 2x/\omega$:

$$R_{kp} = \frac{g\alpha^2}{4\pi^2}T^2 \qquad (21)$$

Thus for typical values $\alpha = 1/50$ and $T = 10$ min R_{kp} equals to 10 min. It proves that tsunami non-breaking is quite common. (This conclusion is confirmed further for predictable tsunami waves in the Far East of the USSR.) Within the linear theory the solution can be extended to the dry zone case. With total depth reduced to zero a criterion of the smooth solution of Eq. (8) can be obtained in the form $Br < 0.65$. This criterion results from the formula given in [13] and differs by 30% from condition (20). It shows once more that using the linear approach when analyzing the tsunami run-up is possible.

The observational data attest that if after tsunami a group of waves comes to the shore the maximal of them are the second to fifth [14,15]. There are also data and predictions attesting that in the open ocean tsunami waves also propagate in groups [16,17,18,19]. It proves the possibility of using partial quasi-monochromatic solutions for analysis and prediction of tsunami elements in the coastal zone. In practice the knowledge of tsunami dynamic characteristics (level shifting, flow velocity) in the sea and on the beach is necessary for the estimation of tsunami hazard for hydrotechnical and coastal constructions. It is easier to take the wave parameters

for the beach than for the open sea since the open sea data are extremely scanty if any. These parameters can be obtained from the analysis of the tsunami behavior on the beach described in catalogues [14,15]. This kind of an approach to calculating tsunami elements was set forth in [20]. If the run-up height and tsunami flooding duration or the tsunami period are known we can transforms solutions (5) and (11) with regard to (20):

$$\begin{aligned} \eta &= -J_0(\sigma)\sin\lambda - \frac{2Br}{\sigma^2}J_1^2(\sigma)\cos^2\lambda, \\ u &= -\frac{2}{\sigma}J_1(\sigma)\cos\lambda, \\ x &= -J_0(\sigma)\sin\lambda - \frac{2Br}{\sigma^2}J_1^2(\sigma)\cos^2\lambda - \frac{\sigma^2}{4Br}, \\ t &= \lambda + \frac{2Br}{\lambda}J_1(\sigma)\cos\lambda \end{aligned} \qquad (22)$$

where $J_1(\sigma)$ is the Bessel function. These solutions are given in the closed form. But their immediate application is difficult because of their implication. There are numerical solutions for the periodic tsunami transformation process on a sloping beach. In the analytic form it is possible to obtain the extrema of the time functions η and u. These functions define the maxima of up and down level shifts and run-up and run-down velocities. The details of the calculations [21] are omitted and the level shifting extrema formula is given in the parametric form,

$$\eta_{extr} = \pm J_0(\sigma), \quad x = \eta_{extr} - \frac{\sigma^2}{4Br}. \qquad (23)$$

In Fig. 1 the calculation results for Eq.(23) are given. With rather small values of Br in the region $x > -1/2Br$. Eq. (23) gives simple asymptotic formulae:

$$\begin{aligned} \eta_{max} &= \frac{1+Br\cdot x}{1+Br}, \\ \eta_{min} &= \frac{1+Br\cdot x}{1+Br}. \end{aligned} \qquad (24)$$

Thus for non-breaking waves the run-up height is equal to the run-down depth. From

$$x_* = -\sigma_*^2/4Br, \qquad (25)$$

(where $\sigma_* = 2.45$ is the first zero of the function $J_0(\sigma)$) run-up levels decrease monotonically. The value x_* can be identified with the width of the coastal zone where the tsunami danger is considerable. This characteristic is very important and formula (25) is given in the dimensional form,

$$\frac{h_*}{R} = \frac{\sigma_*^2}{4Br}. \tag{26}$$

Here h_* is the maximum basin depth down to which taking into account the tsunami effect is necessary.

Similar formulae can be obtained for the extreme of the flow velocity (Fig. 2) [21]. The absolute maximum of velocity is reached on the moving shoreline:

$$u = 1 \text{ with } x = -Br/2. \tag{27}$$

or in the dimensional variables

$$u=\omega R/\alpha. \tag{28}$$

(The same result can be easily obtained within the linear theory [13]). The maximum of velocity proves to be 5 m/sec with $R = 10$ m and the period of 20 min on the slope with $\alpha = 1/100$. It is reached at the depth of 1.25 m. Note that the maxima of run-up and run-down velocities coincide. In this paper only two formulae for the maximal values of the flow velocity [21] on the dry shore are given (the exact formula):

$$u_{extr} \sim \pm\left(1+\frac{Br}{2}x\right). \tag{29}$$

In the sea $-Br \ll x < -Br/2$ with rather small Br,

$$u=\pm\sqrt{\frac{2}{Br}\sqrt{\frac{1}{Br}+\frac{2x}{Br}}+1 - \frac{2x}{Br} - \frac{2}{Br^2}}. \tag{30}$$

These formulae give the complete description of changing of periodic waves parameters on a plane slope. In practice a tsunami wave represents a finite wave train. If the length of a wave train is limited it results naturally in "blurring" of the wave field nodes and field antinode lessening. The exact solutions can be formally obtained by superposition of the particular solutions similar to (11),

$$\phi(\sigma,\lambda) = \int A(\Omega)\, J_0(\Omega\sigma)\, \cos[\Omega\lambda - \psi(\Omega)]d\Omega \tag{31}$$

If the wave source is rather distant from the shore the constants A and ψ are determined through the Fourier spectrum of the incident wave. Some particular solutions are formed this way in [8, 22, 23, 24]. The calculations are so complicated that they prompted the authors of review [12] to say that the basic contribution in [8] is the demonstration that in the non-linear long-wave approximation there are elevation waves propagating without breaking on a permanent sloping beach, rather than the run-up calculation. Nevertheless a simple calculation procedure to obtain the maximum run-up can be suggested. The water boundary motion is found in account

with transformations (5):

$$x = \frac{1}{4Br}\left(\int \Omega\, A(\Omega)\, \sin(\Omega\lambda - \psi)d\Omega - \frac{1}{2}\left[\int \Omega^2 A(\Omega)\, \cos(\Omega\lambda - \psi)d\Omega\right]^2\right) \qquad (32)$$

The maximum run-up is determined by the maximum of only the first component (the second component is u^2 and in the maximum $u = 0$). thus

$$x_{extr} = \frac{1}{4Br}\, extr \int \Omega\, A(\Omega)\, \sin(\Omega\lambda - \psi)d\Omega, \qquad (33)$$

Within the linear theory Eq. (33) describes the maximum of the wave height on the shoreline [9,13]. Therefore the "linear" approach to finding the maximum levels of water elevation on the shore for the arbitrary form of the tsunami wave is verified. Of interest is to compare the specific run-up height value for different forms of tsunami waves. Similar to Eq. (18) the formula for the vertical run-up can be given in dimensional variables:

$$\frac{R}{H_0} = \sqrt{\frac{L_\omega}{\lambda}}\, m, \qquad m = 2\sqrt{\pi}\, extr \int \sqrt{\Omega}\, \zeta(\Omega) \exp\left[i\left(\Omega\lambda - \delta + \frac{\pi}{4}\right)\right]d\Omega \qquad (34)$$

where ζ is the dimensionless amplitude spectrum and δ is the phase spectrum of the incident tsunami wave with the height H_0 and length λ at the distance L_ω from the shoreline. For the monochromatic wave $m = 2\pi\sqrt{2} = 8.9$. Different types of pulse perturbation run-up are considered in [13]. In this paper we give only one solution corresponding to the single perturbation wave run-up:

$$\eta_{\text{на}\Delta}(t) = \frac{H_0}{1 + (2t/T)^2} \qquad (35)$$

In this case calculation (34) leads to

$$m_+ = \pi\sqrt{2}\left(\cos\frac{\pi}{10}\right)^{5/2} \approx 4.4, \quad m_- = -\pi\sqrt{2}\left(\cos\frac{3\pi}{10}\right)^{5/2} = -0.23.$$

Here m_+ corresponds to the run-up and m_- to the run-down of the tsunami wave. (Compare the values of m for the elevation wave of the sine pulse type $m_+ = 3.9$ and $m_- = -1.4$ [13]). Thus the motion of a single elevation wave leads not only to tsunami run-up but also to the following run-down with the run-down depth about 30% of the run-up height. It should be also stressed that run-up value depends on the shape of the wave and this must be taken into consideration when analyzing laboratory experiments data. At the same time it is possible to use $m_+ = 5$ for rough tsunami zonation calculations [13,25].

These formulae give the complete description of the tsunami run-up on the sloping beach. In case the beach has complex configuration the solutions of he nonlinear problem in the explicit form are not obtained. Nevertheless the given

verification of the linear theory for the run-up of tsunami waves with rather distant sources makes it possible also to investigate the tsunami run-up in these cases since the linear problem is solved for many laws of depth changing [12,26,27]. Therefore we can considerably expand the framework of the theory for the non-breaking tsunami run-up on the beach. Only one solution (in dimensional variables) is given here. It corresponds to the monochromatic wave run-up on the beach conjugate with an even bottom at the distance L_ω from the shoreline [13,26]:

$$\frac{R}{H_0} = \frac{2}{\sqrt{J_0^2(4\pi L_\omega/\lambda)+J_1^2(4\pi L_\omega/\lambda)}} \tag{36}$$

This solution can be easily approximated by simple dependencies:

$$\frac{R}{H_0} = \begin{cases} 2, & L_\omega<0.05\lambda, \\ 2\pi\sqrt{2L_\omega/\lambda}, & L_\omega>0.05\lambda. \end{cases} \tag{37}$$

Fig. 3 shows the relative heights of the run-up, obtained from these formulae. The first line is for (36) and the second one is for (37). The linear approach is verified for rather distant sources only, i.e., with great L_ω/λ and this fact should be taken into account. Otherwise the linear theory can lead to miscalculations of the run-up height: the exact solution of the nonlinear problem with $L_\omega = 0$ (the vertical wall) gives run-up values greater than in the linear case:

$$\frac{R}{H} = 4\left(1+\frac{H_0}{h}=\sqrt{1-\frac{H_0}{h}}\right). \tag{38}$$

In conclusion we can give the 100 years prediction for the tsunami dynamic characteristics on the Kurils shore: the maximum stream velocity, breaking parameter, maximum level elevation on the shoreline and critical run-up height corresponding to wave breaking [3,28]. They were calculated by the period and run-up height [29,30]. We made use of formulae (20), (21, (23), (28). These data are tabulated. It is evident from the table that practically all $Br < 1$ are smaller than unity. Therefore in these regions one can expect quiet flooding on the beach and other tsunami effects in predicted characteristics. Near Severo-Kurilsk $Br > 1$ is greater than unity; hence tsunami waves are likely to break here. This situation was observed on 4-5 November 1952 when waves with abrupt front ran up on Severo-Kurilsk. Methods of calculating tsunami effects with $Br > 1$ greater than unit need further verifying and this case is not tabulated. The data on the characteristics of the tsunami waves far from the shore also are not given since for the analysis of tsunami behavior in gulfs and bays it is necessary to take into account the resonance effects caused by two-dimensionality of the problem. But tsunami behavior on the dry shore is described by the one-dimensional theory and the given data are more reliable. The large-scale tsunami zonation with regard to the two-dimensional effects is already under way. The practical experience of the Yuzhno-Kurilsky Bay tsunami zonation accomplished near Yuzhno-Kurlisk is described in [3].

REFERENCES

1. T.V. Martynenko, V.V. Yakovlev. Single wave diffraction on bodies of revolution. In: TsunamiConference, Digest of Reports. Obninsk, 1985, p. 148-150. (in Russian)

2. S.L. Solovyov. Tsunami Defense. Priroda, 1981, N. 5, p. 54-67. (in Russian)

3. V.M. Kaistrenko, Ye.N. Pelinovsky, K.V. Simonov. Prediction of tsunami run-up type on Kuril-Kamchatka zone Coast. Ibid., p. 78-80. (in Russian)

4. V.M. Kaistrenko, Y.N. Pelinovsky, K.V. Simonov. Tsunami Wave parameter calculation in the shallow-water zone and on the shore. In: Problems of Hydromechanics in the Use of the Ocean, P.2 A.Kiev, the Institute of Hydrophysics of the Ukrainian Academy of Sciences. 1984, p. 112-113. (in Russian)

5. Ch. Goto. Nonlinear long waves in a channel of variable section. -Coast. Eng. Japan, 1974, v. 17, p. 1-12.

6. J.A. Battjes. Surf similarity. -In: Proc. 14th Coast. Eng. Conf. Copenhagen, 1974, p. 466-480.

7. A.J. Bowan. Wave-wave interactions near the shore. Lect. Notes Phys., 1977, v. 64, p. 102-113.

8. G.F. Carrier, H.P. Greenspan. Water waves of finite amplitude on a sloping beach. -J. Fluid Mech., 1958, v. 4, N 1, p. 97-109.

9. R.Kh. Mazova, Ye.N. Pelinovsky, S.Kh. Shavratsky. One-dimensional theory of nonbreaking tsunami climbing a beach. In: Processes of tsunami generation and propagation. Moscow, the Institute of Oceanography of the USSR Academy of Sciences, 1983, p. 98-103. (in Russian)

10. M. Brandsma, D. Divoki, L.S. Hwang. Circum-pacific variations of computed tsunami features. - Manuscript Report Series, N. 48, Ottawa, 1978, p. 132-151.

11. A.W. Garsia, J.R. Houston. Tsunami run-up predictions for Southern California coastal communities, USA. -Bull. Roy. Soc. New Zealand, 1976, N 15, p. 5-18.

12. B. Le Mehaute, C. Koh, L.S. Hwang. A synthesis of wave run-up. J. Waterways Harb. Div., ASCE, 1968, v. 94, N 1, p. 77-92.

13. R.Kh. Mazova, Ye.N. Pelinovsky. The linear theory of tsunami climbing a beach. In: Izv.Akad.Nauk SSSR, Fiz.Atm. i Okeana, 1982, v. 18, N. 2, p. 166-171. (in Russian)

14. S.L. Solovyov, Ch.N. Go. The Catalogue of tsunamis on the west coast of the Pacific Ocean. Moscow, Nauka, 1974, 310 p.

15. S.L. Solovyov, Ch.N. Go. The catalogue of tsunamis on the East Coast of the Pacific Ocean. Moscow, Nauka, 1975, 203 p. (in Russian)

16. B.D. Dykhan, V.M. Zhak, Ye.A. Kulikov et al. The first registration of tsunami in the ocean. (The 23 February 1980 tsunami at the South Kuril Isles). In: Dok. Akad. SSSR. 1981, v. 257, N 5, p. 1088-1092 (in Russian)

17. V.V. Ivanov. Space-time evolution of an earthquake and tsunami generation. Tsunami Conference, Digest of Reports, Gorky, IAP, the USSR Academy of Sciences, 1984, p. 73-75. (in Russian)

18. V.V. Ivanov, K.V. Simonov, O.I. Gardner. Evaluation of screening effects and tsunami danger of bays. In: Izv.Akad.Nauk SSSR. Fiz.Atm.i Okeana, 1984, v. 20, N 12. p. 1206-1214. (in Russian)

19. V.N. Mitrofanov, Ye.A. kulikov, V.A. Dzhumagaliev, N.L. Makovsky. The 24 March 1984 Iturup Tsunami. In: tsunami Conference, Digest of Reports. Gorky, IAP, the USSR Academy of Sciences, 1984, p. 115-117. (in Russian)

20. V.M. Kaistrenko, Ye.N. Pelinovsky, K.V. Simonov. Calculation of coast defence and hydrotechnical constructions with tsunami taken into account. In: Tsunami Conference, Digest of Reports. Gorky, IAP, The USSR Academy of Sciences, 1984, p. 76-78. (in Russian)

21. V.M. Kaistrenko, Ye.N. Pelinovsky, K.V. Simonov. Run-up and transformation of tsunami waves on shallow water. Meteorologiya i gydrologiya, 1985, N 10, p. 68-75. (in Russian)

22. R.Kh. Mazova, Ye.N. Pelinovsky, S.Kh. Shavratsky. The nonlinear theory of tsunami climbing a beach. In: Waves and Diffraction, v. 2. Moscow, IRE of the USSR Academy of Sciences, 1981, p. 277-280. (in Russian)

23. N. Shuto. Standing waves in front of a sloping dike. Coast. Eng. Japan, 1972, v. 15, p. 13-23.

24. L.O. Spielvogel. Run-up of single wave on a sloping beach. J. Fluid Mech., 1976, v. 74, N 4, p. 685-694.

25. Ye.N. Pelinovsky. Nonlinear Dynamics of Tsunami Waves. Gorky. IAP, the USSR Academy of Sciences, 1982, 226 p. (in Russian)

26. S.I. Kozlov. Tsunami climbing a beach without breaking. In: Izv.Akad.Nauk SSSR, Fiz.Atm.i Okeana, 1984, v. 20, N 6, 14p. (in Russian)

27. R.Kh. Mazova. Tsunami wavesclimbing sloping beaches with complex profiles. In: Short-Term and Long-Term Tsunami Prediction. Moscow, Institute of Oceanography of the USSR Academy of Sciences, 1983, p. 58 (in Russian)

28. Ch.N.Go, V.M. Kaistrenko, Ye.N. Pelinovsky, K.V. Simonov. Practical tsunami zonation. In:SeismicDanger Prediction in the Far East. Yuzhno-Sakhalinsk, 1984, p.9-11. (in Russian)

29. Ch.N.Go, V.M. Kaistrenko, K.V. Simonov. Local Long-Term tsunami Prediction and Tsunami Zonation. Preprint. Yuzhno-Sakhalinsk, Sakhalin Complex Scientific Research Institute, the Far East Scientific Centre of the USSR Academy of Sciences, 1982, 26 p. (in Russian)

30. Ch.N. Go, V.M. Kaistrenko, K.V. Simonov et al. Calculation methods for coastal tsunami danger. In: Earthquakes and Hazard Warning. Proc. of the Geological Congress, v.6. Moscow, Nauka, 2984, p.133-140. (in Russian)

PREDICTION OF THE TSUNAMI DYNAMIC CHARACTERISTICS ON THE KURILS ZONE SHORES

Point	Slope of the Bottom	Period min	Run-up m	Critical Run-Up Height m	Height on the Shoreline, m	Flow Velocity m/sec	Br
Isl. Paramushir (Severo-Kurlisk)	$0.33*10^{-2}$	30	17.8	9	--	--	2.0
Isl. Matua	$1.25*10^{-2}$	18	9.9	45	8.3	4.6	0.2
Isl. Simu-simushir (The northern part)	$2.5*10^{-2}$	16	8.6	143	8.1	2.2	0.06
Isl. Urup (Kastrikum Cape)	$1.25*10^{-2}$	26	8.2	9	7.5	2.6	0.1
Isl. Urup (Van-der-Lind Cape)	$2.5*10^{-2}$	20	6.8	223	15.3	3.5	0.1
Isl. Iturup (Kasatka Bay)	$1.7*10^{-2}$	24	7.5	894	7.1	1.9	0.05
Isl. Kunashir (Yuzhno-Kurilsk)	$1.25*10^{-2}$	20	6.8	56	6.2	2.9	0.1
Isl. Shikotan (Malo-kurilskaya Bay)	$1.25*10^{-2}$	20	6.8	56	6.2	2.9	0.1

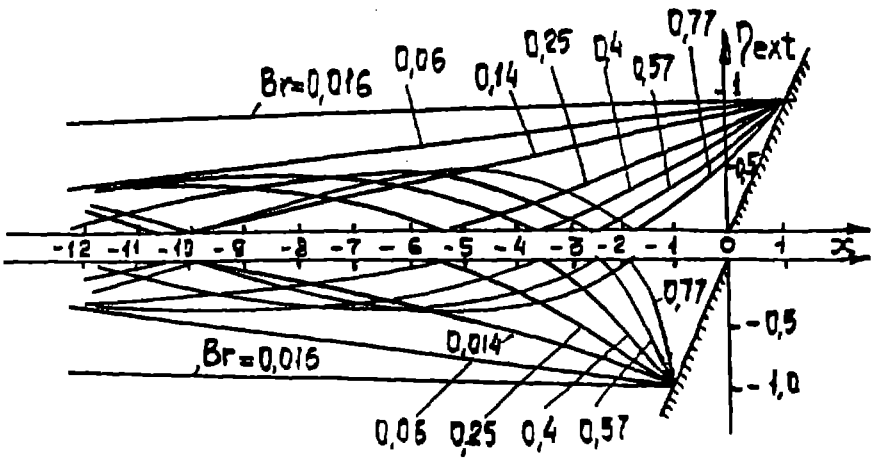

Figure 1. Extrema values of surface elevation as function of distance from shoreline (Equation 23).

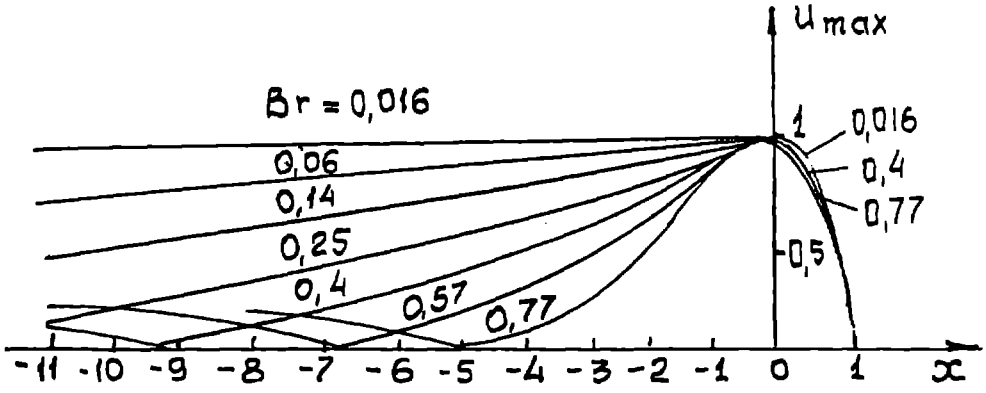

Figure 2. Maximum flow velocities as a function of distance from shoreline.

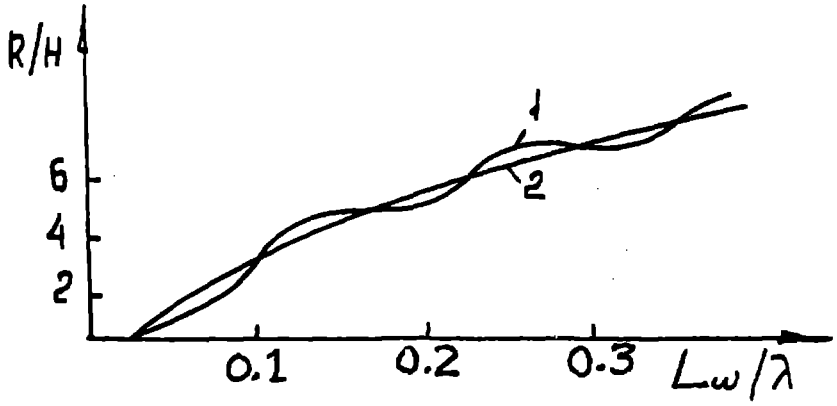

Figure 3. Run-up as a function of distance from shoreline. Line 1 is from equation 36; line 2 is from equation 37.

APPLICATION FOR MEMBERSHIP

THE TSUNAMI SOCIETY
P.O. Box 8523
Honolulu, Hawaii 96815, USA

I desire admission into the Tsunami Society as: (Check appropriate box.)

☐ Student ☐ Member ☐ Institutional Member

Name _____ Signature _____

Address _____ Phone No. _____

_____

Zip Code _____ Country _____

Employed by _____

Address _____

Title of your position _____

FEE: Student $5.00 Member $25.00 Institution $100.00

Fee includes a subscription to the society journal: SCIENCE OF TSUNAMI HAZARDS.

Send dues for one year with application. Membership shall date from 1 January of the year in which the applicant joins. Membership of an applicant applying on or after October 1 will begin with 1 January of the succeeding calendar year and his first dues payment will be applied to that year.